Master's thesis

NTNU
Norwegian University of Science and Technology
Faculty of Engineering
Department of Mechanical and Industrial Engineering

Erik Fjeldstrøm Trydal

Development of an Additively Manufactured Payload Mounting Solution for the HYPSO-2 6U CubeSat

Master's thesis in Mechanical Engineering
Supervisor: Antoine B. Rauzy
Co-supervisor: Evelyn Honoré-Livermore
June 2022

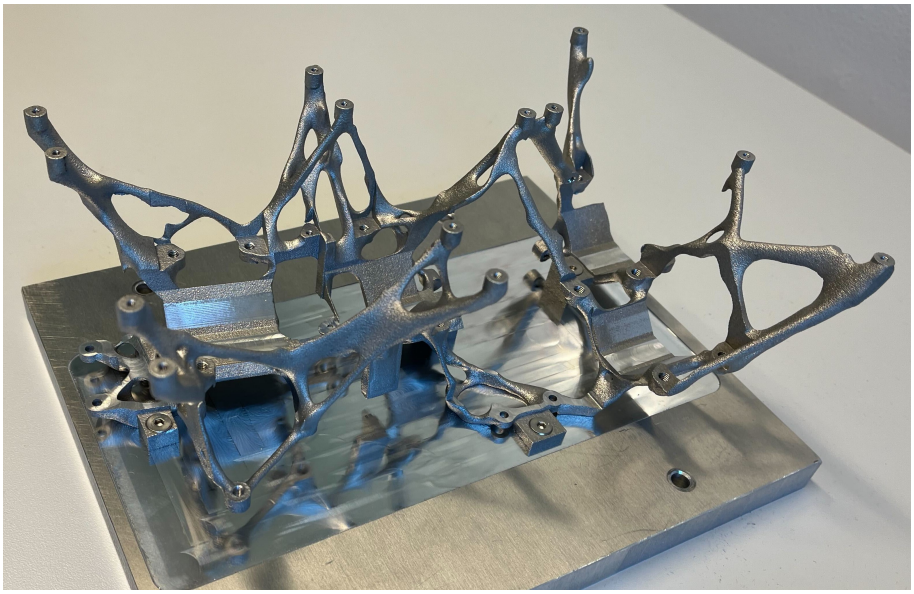

NTNU
Norwegian University of
Science and Technology

Erik Fjeldstrøm Trydal

Development of an Additively Manufactured Payload Mounting Solution for the HYPSO-2 6U CubeSat

Master's thesis in Mechanical Engineering
Supervisor: Antoine B. Rauzy
Co-supervisor: Evelyn Honoré-Livermore
June 2022

Norwegian University of Science and Technology
Faculty of Engineering
Department of Mechanical and Industrial Engineering

NTNU
Norwegian University of
Science and Technology

Abstract

The main focus of this thesis is on the development of an additively manufactured mounting solution for the HYPerspectral Smallsat for Ocean observation (HYPSO)-2 payload as a part of the HYPSO project at Norwegian University of Science and Technology (NTNU). The main purpose of the work presented is to evaluate the feasibility of using additive manufacturing in CubeSats and to see what performance increases the addition of this manufacturing technology can bring to the project.

When developing the part topology optimization was used to leverage the design freedom gained from additive manufacturing. This optimization process started with function integration where the design space to be optimized was created. Then, the topology optimization simulations were done to generate lower and lower mass concepts. This was followed by simulations of the generated concepts to find areas of improvement for manual changes.

The resulting part from this optimization process met the requirements for the simulated values while reducing the weight by 81.5% compared to the HYPSO-1 design. This shows that additive manufacturing can enable great performance increases, especially in terms of mass reduction, as long as the associated risks are managed. As mass reduction is of high importance for satellites this manufacturing technology therefore shows great promise in the development of CubeSats.

Sammendrag

Hovedfokuset i denne oppgaven er på utviklingen av en additivt produsert monteringsløsning for HYPerspectral Smallsat for Ocean observation (HYPSO)-2 nyttelasten som en del av HYPSO-prosjektet ved Norges Teknisk-Naturvitenskapelige Universitet (NTNU). Hovedformålet med arbeidet som presenteres er å evaluere muligheten for å bruke additiv produksjon i CubeSats og å se hvilke ytelsesøkninger innføringen av denne produksjonsteknologien kan gi prosjektet.

Under utviklingen av delen ble topologioptimalisering brukt for å utnytte designfriheten additiv produksjon tillater. Denne optimeringsprosessen startet med funksjonsintegrasjon hvor designrommet som skulle optimaliseres ble laget. Deretter ble topologioptimaliseringssimuleringene gjort for å generere konsepter med lavere og lavere masse. Til slutt ble konseptene simulert for å finne forbedringsområder for manuelle endringer.

Den resulterende delen fra denne optimaliseringsprosessen oppfylte kravene til de simulerte verdiene samtidig som det nye designet reduserte vekten med 81,5% sammenlignet med HYPSO-1-designet. Dette viser at additiv produksjon kan muliggjøre store ytelsesøkninger, spesielt når det gjelder massereduksjon, så lenge de tilknyttede risikoene håndteres. Siden massereduksjon er av stor betydning for satellitter, er denne produksjonsteknologien lovende i utviklingen av CubeSats.

Preface

The work presented in this thesis has been conducted as part of the HYPSO project at the NTNU SmallSat Lab, for the Department of Mechanical and Industrial Engineering in collaboration with the Faculty of Information Technology and Electrical Engineering at NTNU. This thesis is the result of five months of work done in the spring of 2022, and builds further on the specialization project that was done in the fall of 2021 in preparation for this thesis.

I would like to than my supervisor, Professor Antoine Rauzy, and co-supervisor, Evelyn Honoré-Livermore, for the support and guidance they have given me while working on the thesis and specialization project. I would also like to thank everyone in the HYPSO project, especially Anders Brørvik, Jonas Brunsvik and Marie Henriksen, for providing me with support, excellent discussions and a good work environment.

Acronyms

AM Additive Manufacturing. 1, 6–9, 35

CAD Computer-aided Design. 12

DfAM Design for Additive Manufacturing. vi, 6, 7, 12

DTM Design Theory and Methodology. 6, 7

FEA Finite Element Analysis. 10, 12

HSI Hyper Spectral Imager. 2, 13–15, 17, 18, 34

HYPSO HYPerspectral Smallsat for Ocean observation. i, 1, 2, 4, 5, 12, 31, 34

IMU Inertial Measurement Unit. vi, 2, 14, 16

NTNU Norges Teknisk-Naturvitenskapelige Universitet. i

NTNU Norwegian University of Science and Technology. i, ii, 1, 4

PBF Powder Bed Fusion. vi, 5, 6, 8, 9

RGB camera Red Green Blue Camera. vi, 2, 3, 13, 15–17, 26, 33, 34

SIMP Solid Isotropic Material Penalization. 11

TO Topology Optimization. vi, 4, 10, 13–16, 18–20, 26, 30, 32, 33, 35

Contents

List of Figures

List of Tables

1 Introduction

1.1 The HYPSO mission

The HYPerspectral Smallsat for Ocean observation (HYPSO) mission will primarily be a science-oriented technology demonstration project. It will enable low-cost, high-performance hyper-spectral imaging and autonomous on-board processing of the ocean color along the Norwegian coast to observe, monitor and predict the oceanography and biology in the observed area. The Norwegian University of Science and Technology (NTNU)'s first science-oriented SmallSat project, HYPSO-1, was launched in January 2022, and is followed by a second mission, HYPSO-2, in 2024. This follow-up mission, HYPSO-2, has the purpose of implementing design changes and improvements for further development of HYPSO-1.

1.2 Problem outline

The aerospace industry is continuously working towards lower weight parts as the cost of launching satellites is heavily reliant on the weight. To reduce the weight of HYPSO-2 Additive Manufacturing (AM) was identified as a possible area to explore for the new design. It is of particular interest for the payload mounting solution as it is believed to have the potential for great weight savings. As AM and CubeSats are both focus areas for NTNU it is also of great interest to check if AM can be successfully utilized in space. This thesis will therefore look at the feasibility and development of a new payload mounting solution for HYPSO-2 where AM is utilized to realize potential improvements in the design. The secondary objective is to create an optimization procedure that can be reused in later development projects at NTNU that involve AM.

R1: Is AM a feasible manufacturing technology to use when developing structural components in CubeSats?

R2: Does topology optimization pose as a good design tool when designing CubeSats?

1.3 Scope

AM is associated with a vast amount of other technologies and techniques. These span from the specific AM processes, like vat photo-polymerization or powder bed fusion, to design technologies, such as topology optimization and lattice structures. This thesis therefore builds on the work done in a specialization thesis, previous work done in preparation for the master's thesis, where it was found that topology optimization and laser powder bed fusion with AlSi10Mg as the material was to be utilized for the master's thesis.

Furthermore it was considered to use thermal simulations to correct for the warping during manufacturing. This however required machine specific information which was not available from the manufacturer. Instead, the part is post-processed using machining to obtain the required tolerances.

2 Background

2.1 The HYPSO-2 satellite

HYPSO-2 follows the CubeSat standard. CubeSats are a type of satellite with a weight up to 30 kg and are based on the standard measuring unit of a 10x10cm cube, called one unit or "1U". It is common to combine several cubes to form the satellite. The standardization of satellites gives the possibility of using commercial-off-the-shelf components and launch with other missions on the same launch vehicle, thus reducing cost and development time. CubeSats therefore provide

low-cost access to space and are often used by researchers, universities, small companies, etc. for education and technology demonstration purposes. HYPSO-1 and HYPSO-2 are 6U CubeSats with six units of 1U, placed in a 2x1x3 (x,y,z) formation.

2.1.1 Current payload design

The design of HYPSO-1 is seen in Figure 1. The coordinate system used in this thesis is also included in the figure, in addition to the direction of "front" and "rear" which is used to denote relative position of parts. The components of interest for this thesis are mainly the optical and mechanical components plus the Inertial Measurement Unit (IMU). The optical components are the Hyper Spectral Imager (HSI) train, i.e. the objectives, sensor, grating and grating cassette, the Red Green Blue Camera (RGB camera), and star tracker. The mechanical components of interest are the HYPSO-1 platform (including cross-links, dampers etc.), mounting brackets and 6U frame. The surrounding components are included to visualize the available space for the HYPSO-2 platform.

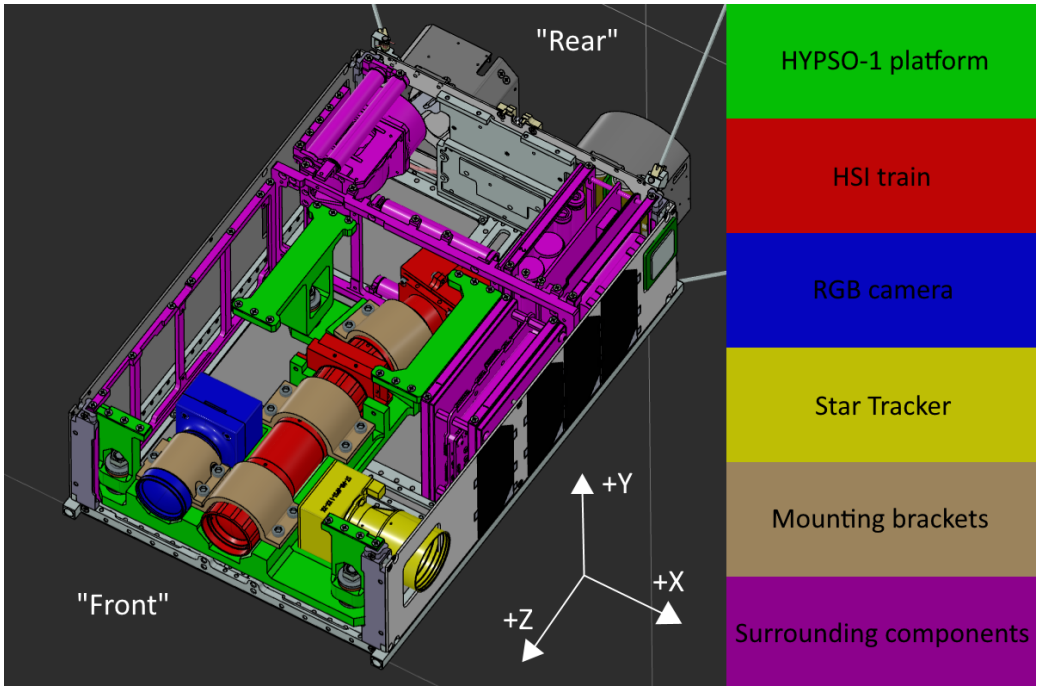

Figure 1: The design of HYPSO-1. The IMU is placed underneath the RGB camera on the underside of the HYPSO-1 platform.

2.1.2 Changes for HYPSO-2

HYPSO-2 incorporates several new parts compared to HYPSO-1. Of those, the new star tracker and RGB camera are of interest to this thesis. The main differences between the old and new RGB camera are the slightly different diameters for the lens and a larger sensor that require more space. For the star tracker the main differences are a longer length and the placement of the fastening holes moving from one side to the back side. A comparison between the new and old parts can be seen in Figure 2.

In addition to the introduction of new parts some old parts will no longer be used. Of note here is that the dampers were deemed unnecessary in a concurrent master's thesis by Anders Brørvik. This frees up the constraints on the design to allow more than four mounting points from the 6U-frame to the platform. This also means that the crosslinks connecting the 6U-frame to the platform will no longer be necessary and can instead be merged into one part.

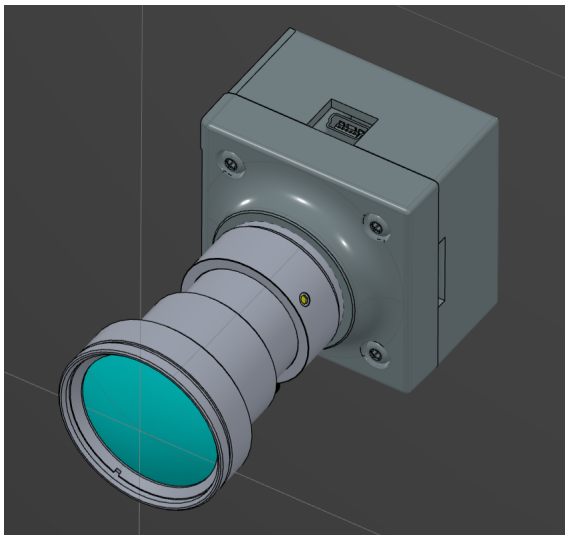

(a) Old RGB camera (82x43x44 mm)

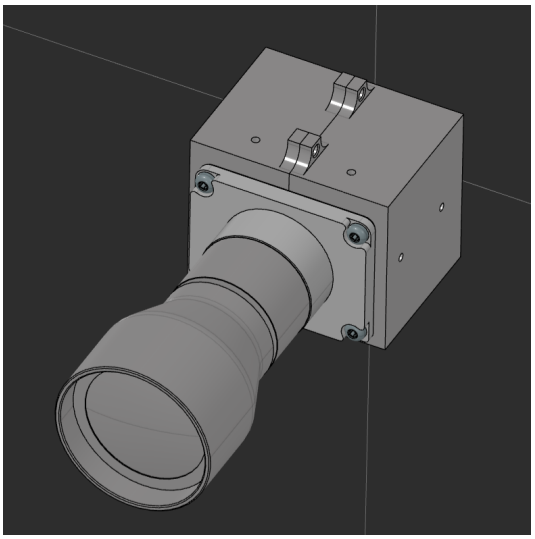

(b) New RGB camera (113x51x49 mm)

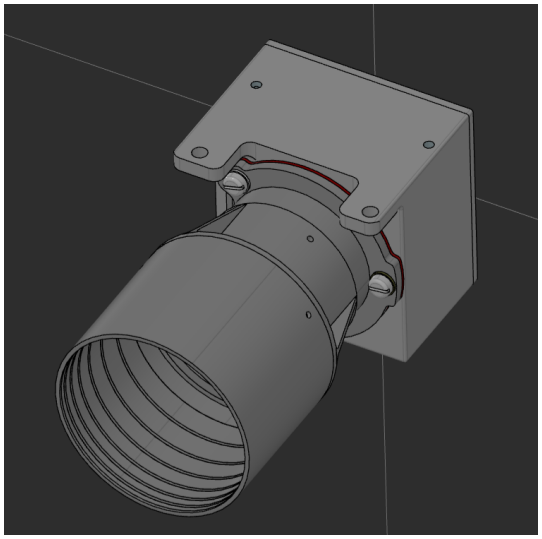

(c) Old star tracker (82x42x40 mm)

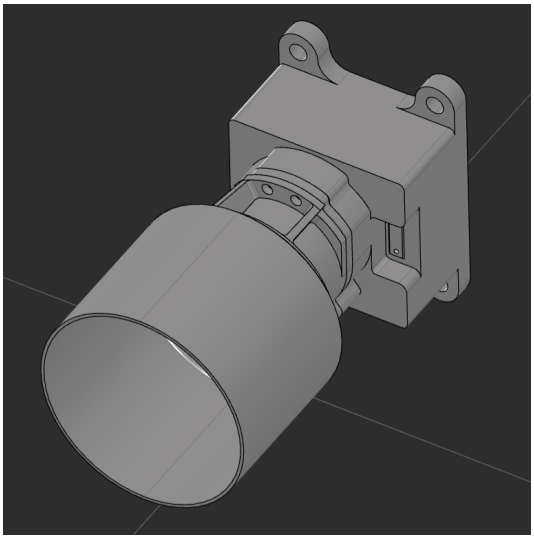

(d) New star tracker (98x60x52 mm)

Figure 2: Comparison between old and new RGB camera and star tracker

2.2 Payload requirements

MC-10: The HYPSO-2 spacecraft shall adhere to the 6U CubeSat Design Specifications CP-6UCDS-1.0, University, 2018

MC-10 is a general requirement to ensure operability in space after transit and has been used to formulate several requirements for the HYPSO-2 satellite. Requirements **STRM-3-020**, **STRM-3-025** and **PLD-3-010** are the requirements created from this document that are relevant to the work in this thesis.

STRM-3-020: The CubeSat center of gravity shall fall within:
X-axis: +-4.5cm Y-axis: +-2cm Z-axis: +-7cm

STRM-3-025: No components shall protrude farther than 6.5 mm normal to the surface from the plane of the rail except on the -Z side

PLD-3-010: The total mass of the payload shall be less than 2500g (TBC)

These requirements stem from the 6U CubeSat Design Specifications CP-6UCDS-1.0, University, 2018. They limit the design choices possible, such as a star tracker that protrudes further than 6.5mm, and necessitates a design that distributes mass in a way that is compatible with the rest of the satellite's mass distribution. This means that the design should have a center of mass close to zero in the X- and Y-directions and significantly forward of the geometric center in the Z-direction as the rest of the satellite will move the center of mass backwards when included.

STRM-3-015: All structures shall withstand the loads from launch. Launch provider: (Falcon 9 TBD)

STRM-3-016: Components should not experience higher stress than 60%(TBD) of its yield strength during transit

ENV-10: Spacecraft component eigenfrequencies shall be over 40 Hz + factor of safety 1.85 (TBC) and within 6dB (TBC) response (falcon 9)

ENV-11: No spacecraft component shall physically interfere with another during shock and vibration testing

ENV-15: Spacecraft components shall survive tested shock with a +/- 6dB (TBC) maximum response

These requirements will be met by analyzing the design and making appropriate changes to facilitate a lower maximum stress, such as removing sharp corners, increasing thickness etc, and by increasing stiffness and room for deformation for vibration and shock resistance. The requirements ensure that the payload survives transit to orbit without damage to any of the components.

STRM-3-005: Mechanical components shall be designed so that they can be manufactured with the chosen manufacturing method

STRM-3-006: Mechanical components should be manufacturable in-house at NTNU

STRM-3-010: Custom tools shall not be necessary for assembly

This is to ensure that the design can be manufactured and assembled and will impact design choices. The design space is particularly affected by this requirement as there must be room for post-processing machinery, such as a CNC-tool, and standard tools such as wrenches and Allen keys. It also impacts the TO simulations as manufacturing constraints may be utilized to ensure manufacturability of the generated design.

HSI-4-030: HSI payload keystone should be less than 1 pixel (TBC) within the region of interest (TBD) after correction

HSI-4-065: Stray light should be minimized (method TBD) in the HSI payload design

HSI-4-075: HSI total spectral tilt (including tilt from rotated slit) should be less than 1 pixel

HSI-4-080: HSI decentering should result in less than (TBD) pixels shift (i.e. movement of lenses without tilting)

ENV-25: Spacecraft components shall operate within -20 to 50 °C (TBC) in vacuum environment

ENV-26: The spacecraft subsystem shall survive -30 to 60 °C (TBC) environment in vacuum

These requirements will be fulfilled as long as the design does not introduce any significant deformations during the lifetime of the satellite. This means that the structural components cannot yield at any point, and that temperature fluctuations introduce minimal deformations. Rotations of HSI components relative to each other is particularly undesirable. The design should therefore comply with the HSI requirements in the -20 to 50 °C and not introduce any permanent deformations in the -30 to 60 °C range.

RGB-4-020: The RGB shall be placed with it's axis parallel to the HSI train axis

RGB-4-020 is to ensure that the HSI and RGB point at the same location. Similarly to the HSI it is therefore undesirable that the design alters the angle between the two axis, typically from thermal deformations.

2.2.1 Load environment

The launch of a satellite is a load heavy environment. The main loads experienced during launch is a combination of acceleration, vibration and shock loads. These are therefore specified by the launch provider so that all payloads in the launch vehicle can be safely transported. As the specific launch provider HYPSO-2 will utilize is still unknown the HYPSO-1 launch provider will be used as reference. This was the Falcon 9 with rideshare.

The acceleration loads experienced on a Falcon 9 are 12g, 7.5g and 7.5g for the three axis. As the direction of HYPSO-2 during launch is unknown all axis need to withstand the 12g load. The two other loads are random vibration and shock. Random vibration is accounted for by specifying a minimum eigenfrequency, which for Falcon 9 is 40Hz. A factor of safety of 1.85 is used for the eigenfrequency, resulting in a minimum eigenfrequency of 74Hz. When it comes to shock the system should survive shock loads of 450g.

2.3 Additive Manufacturing

Additive manufacturing is defined by *ISO/ASTM 52900:2015(E) Additive manufacturing — General principles — Terminology* 2015 as a "process of joining materials to make parts from 3D model data, usually layer upon layer, as opposed to subtractive manufacturing and formative manufacturing methodologies". The most common technologies include vat photopolymerization, binder jetting, direct energy deposition, material jetting, material extrusion, and powder bed fusion with several subcategories for each.

Powder Bed Fusion (PBF), depicted in Figure 3, is a process where either a laser or an electron beam is used as a heat energy source for sintering or melting of powder particles to additively manufacture a part layer by layer, Dev Singh et al., 2021. The process starts by spreading a thin layer of fine powder over the build area, which is then bonded to the substrate by the heat energy

source at specified areas. Then a piston lowers the build area slightly to make room for a new layer and a roller or rake evenly distributes a new layer of powder. The process is then repeated to build a part layer upon layer.

Selective laser melting is a type of PBF process that uses a laser to melt the powder fully and fuse each layer to the previous. This process produces very solid and homogeneous parts with excellent mechanical properties. This comes at the cost of a higher power demand and increased thermal stresses. The process also requires an inert gas environment to prevent oxidation. Selective laser melting is very versatile and can be used on a wide range of materials and is the predominant AM process for metal AM, especially in high performance industries such as automotive, medical and aerospace.

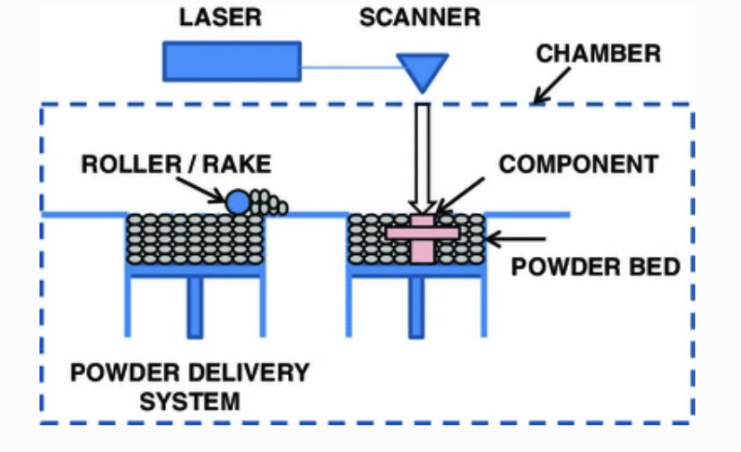

Figure 3: A generic PBF system, Frazier, 2014

2.4 Design for Additive Manufacturing

The process of adding layer upon layer enables a high degree of design freedom compared to traditional manufacturing technologies and has the potential for complex geometry without adding significant additional cost, Durakovic, 2018. This is because the interior part of the geometry is accessible and complex geometry is easily made when done on a 2D-layer one at a time, Gibson et al., 2021. This makes AM suitable for computer generated designs, such as topology optimization or similar tools, where significant weight and performance improvements can be made with little to no additional cost, despite the increased geometric complexity. This means that Design for Additive Manufacturing (DfAM) is very different from other Design for X methodologies.

2.4.1 Methodology

Because designing for AM has a lot fewer restrictions compared to traditional manufacturing the design methodology is significantly different. It is also an emerging research field, so there is currently no consensus on what the preferred methodology for AM is. According to Yang and Zhao, 2015 the proposed methodologies for AM can be sorted into two categories; The first is AM methodologies centered around AM-enabled structure optimization design methods, i.e. methods centered around topology optimization or similar optimization tools, and the second focuses on DfAM methodologies.

The first category is usually employed when concrete optimization objectives should be met, such as optimizing for weight, stiffness, compliance and manufacturability, and is usually relatively straight forward and simple. Often methodologies from this category is used to redesign a part, where an existing part is redesigned to be additively manufactured so that optimization can be done. Alternatively, the part is designed based on traditional Design Theory and Methodology (DTM) methods and then optimization is done to improve performance. This type of methodo-

logy therefore generally do not involve AM design considerations outside the specific part being optimized, but rather rely on the standard DTM methods for the product design and add an optimization methodology at the end of the design process for that specific part.

The second category on the other hand has comprehensive and systematic design methodologies that keep AM design considerations and opportunities in mind during the whole design process of the product. This enables product designs that would otherwise not be possible using the traditional manufacturing and assembly constraints from DTM. It also allows central AM considerations such as manufacturing direction, microstructure, geometry, manufacturing volume and manufacturing time to be considered from an early stage in the design process.

Yang, Tang et al., 2015 proposes a DfAM methodology that is seen in Figure 4. This method takes design specifications and process constraints and uses them to give a redesigned structure. The first step of the process is taking the initial design and performing part consolidation according to the functional and performance requirements of the product. This step is named Function integration. A part of this process is to define the functional surfaces, and then find the functional volume that connects them to prepare for the next step. By first locating the surfaces necessary for all the functional requirements the part is not limited by the shape of the initial design. After these surfaces are located they are connected with functional volume, defined as geometry volume added to link functional surfaces to form a solid, which can then be optimized.

The next step is Structure optimization where you apply structure optimization methods on the newly generated design space to achieve a design with better performance. The optimization method and optimization focus and trade-offs are based on the performance requirements of the product. Lastly the design is checked to see that it complies with the functional and performance requirements. If it fulfills the requirements the design solution replaces the initial design with an improved design with fewer parts and/or better performance. If the design solution does not comply with the requirements the process is started anew at the Function integration stage.

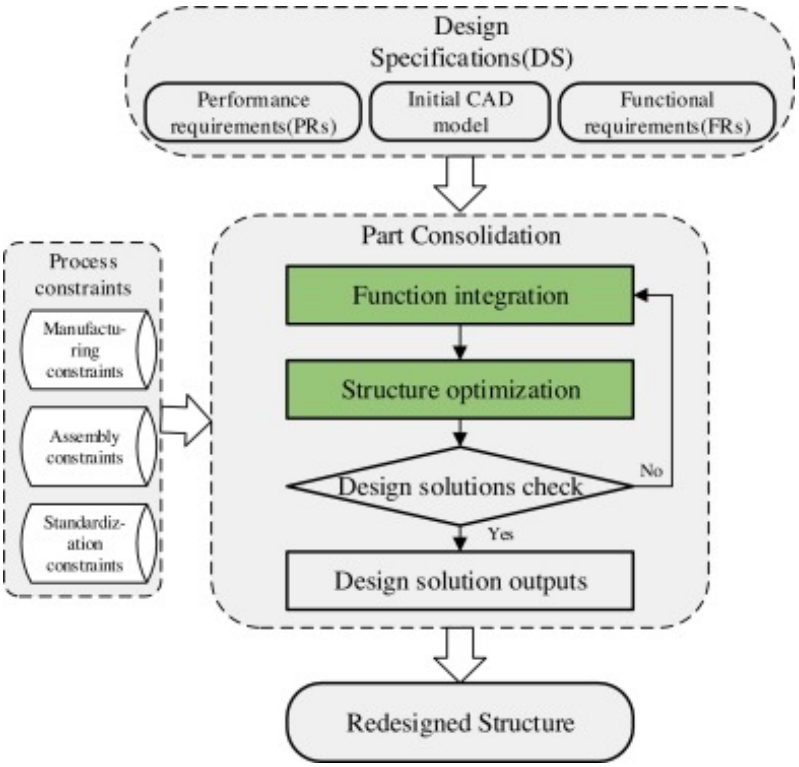

Figure 4: The proposed DfAM methodology by Yang, Tang et al., 2015

2.4.2 General design guidelines

According to Gibson et al., 2021 and Diegel et al., 2019, these are some general design considerations that should be taken into account when designing for AM:

Part orientation is an important variable when additively manufacturing a part. The geometry is generally more accurate in each layer, while surfaces spanning multiple layers often get a jagged surface. A good example of this is a cylinder. If the cylinder is manufactured standing up, then each layer will be a circle. This gives a relatively smooth edge with relatively small layer lines across. If the same cylinder is printed lying down however, then each layer will be a rectangle. This results in a distinct stair-step layer structure for the cylinder, reducing the surface quality of the print. This effect is depicted in Figure 5.

A different consideration is build time. If the previously mentioned cylinder is significantly longer than it is wide, then the amount of layers required will be higher for the vertically printed cylinder than the horizontal one. For technologies that need time to prepare each layer, such as PBF, the additional amount of layers can drastically increase the time needed for production. Part orientation can therefore be a significant contributor to production time.

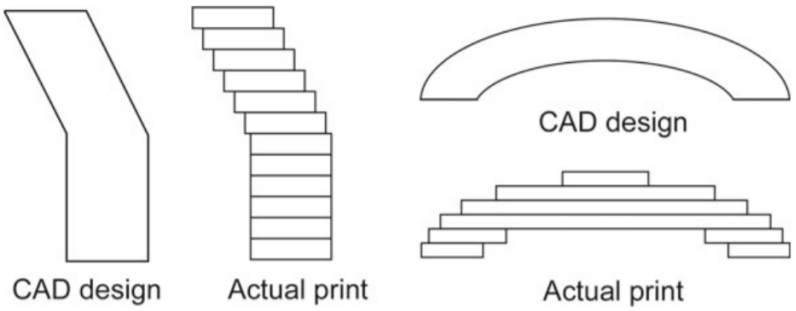

Figure 5: Stair-step effect from layer height, Diegel et al., 2019

Supports are required by some technologies and also require that said support is later removed. Because of this, it is a good idea to design the part in such a way that the use of supports is minimized, and that support is not used in places that are difficult to access. If support is needed in hard to access places, such as the inside of a part, access holes may be needed to remove the support before they are plugged at a later stage. This adds more post-processing, which should be avoided if possible. To minimize support use it is important to consider overhang angle when designing the part. The specific angle varies by technology, but a smaller overhang angle, i.e. more vertical, will remove the need for support. A different build orientation can also be considered to position the geometry more favorably. Some parts might not require support, or much less support, if printed in another orientation as the overhang angle changes drastically from one orientation to another without changing the geometry. This is therefore an easy way to minimize the support usage of the part.

The ease of support removal must be weighed against the support given, as the support can reduce warping in the part and thus hinder the part from hitting the layering mechanism, e.g. the powder-spreading blade, and hinder reduction in dimensional accuracy. It is therefore important to keep the support at areas susceptible to warping.

Hollow part features can be included in the design of additively manufactured parts. Since the AM process enables access to the inside during production it is possible to intentionally add hollow sections to reduce the mass, build time, and material cost of the part. Lattice structures is also an option in cases where additional strength is needed compared to a completely hollow feature

while still retaining most of the reduction in mass, build time and material costs. The downside to hollow features or lattice structures is the need for draining holes to remove the encapsulated powder when using PBF and additional time needed for design. It is therefore necessary to balance the time spent designing to the potential benefits.

Residual stresses need to be accounted for in both the part design and support usage. Residual stresses arise from the contraction of the material as it cools, which can cause delamination of layers, typical of polymer AM, or porosities and cracks, typical of metal AM.

Even thickness of features is a simple way to reduce residual stresses and warping. Especially large solid volumes are prone to high residual stresses and should be avoided. This can be done by for example using lattices or changing the geometry. The uneven distribution of material can also give uneven deformation, which can result in the part warping. Another option to reduce residual stresses is by heat treating the metal. This allows the material to dissipate the stresses and regain most of its original material properties.

2.4.3 Design for metal laser powder bed fusion

When printing polymers using a PBF technology the part generally does not need supports. This is because the powder bed supports the next layer, which then can be printed without any underlying supports. For selective laser melting on the other hand it can be necessary with supports. When unsupported material solidifies it tends to curl upwards, warping the print, which will reduce the quality of the part and potentially hit the layering mechanism.

It also needed for thermal dissipation. If the part is not properly fastened to the substrate, i.e. the plate at the bottom of the powder bed, the cooling rate becomes significantly lower. This results in grain and crystal lattice size differences, particularly in regions far from the substrate, Dilip et al., 2017. The part can later be tempered to change the material properties if desired.

This need for support should therefore be considered when designing the part. One solution is to see if the design can be altered to remove the need for support by for example giving additional or larger contact surfaces with the substrate. Alternatively, the support can be incorporated into a feature so that it does not need to be removed. By incorporating the support the weight is usually increased a little, but in exchange the part gets increased stiffness and less post processing.

2.5 Vibration

Mechanical vibration is an oscillating movement about an equilibrium point. An eigenfrequency, or often called a natural frequency, is the vibration frequency that produces a continuously growing amplitude. This frequency is a function of the stiffness and mass of the structure, where an increase in stiffness increases the eigenfrequency and an increase in mass decreases it. This can be seen in the equation for the eigenfrequency of an undamped spring, $\omega_e = \sqrt{k/m}$, where k is the stiffness and m is the mass connected to the spring. As all structures have one or more eigenfrequencies, it is generally undesirable that the structure experiences vibration close to an eigenfrequency for a prolonged amount of time as the structure can fail, Furger, 2013.

In addition to a specific eigenfrequency, it is also common to use modes to describe eigenfrequency. An eigenfrequency mode is the shape the part or system vibrates in at a specific eigenfrequency. A system with multiple eigenfrequencies will therefore vibrate in different shapes depending on the frequency, as seen in Figure 6. An effective way of improving the eigenfrequency is therefore to look at the corresponding eigenfrequency mode and stiffen or brace the system where the displacement is the largest to disrupt the specific mode shape, thus raising the eigenfrequency.

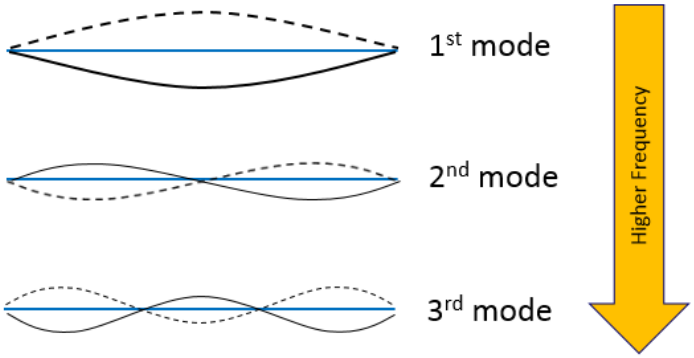

Figure 6: Here the first three mode shapes of a simply-supported beam is shown, *Natural Frequency and Resonance* 2019

2.6 Structural optimization

There are three main types of structural optimization, size optimization, shape optimization and Topology Optimization (TO), Christensen and Klarbring, 2009. In size optimization the design variable is defined as the size of one or more geometry elements, for example the radius of a hole. For shape optimization the design variable is defined as the shape or form of the part. Both of these structural optimization types are technically sub-classes of TO, but due to their differing mathematical implementation they are usually treated as separate methods. A comparison between the structural optimization types can be seen in Figure 7. This thesis focuses on TO.

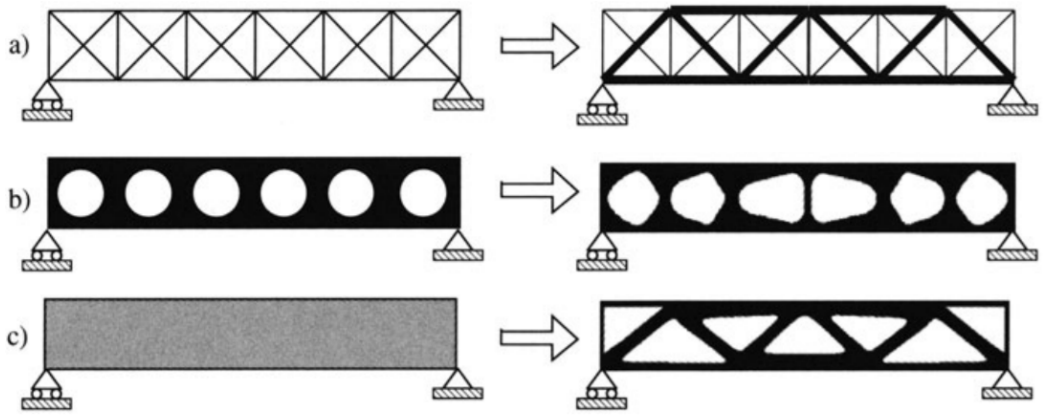

Figure 7: Comparison of structural optimization methods: a) Sizing optimization of truss structure, b) shape optimization of holes, c) topology optimization of a beam. Bendsøe and Sigmund, 2004

2.6.1 Topology optimization

TO is a numerical method used to find an optimal lay-out of the geometry of a part within a given space, Bendsøe and Sigmund, 2004. The space to be optimized is typically defined as a design space and is the area for which the part will not interfere with other surrounding components or functions. Typical simulation inputs include loads, connections, design space and constraints.

Density-based TO is formulated using finite element models. Each element is given a pseudo-density value from 0 and 1, where 0 represents a void and 1 represents a fully solid element, which acts as a design variable to be optimized. The design is then simulated using Finite Element Analysis (FEA) to find displacements and stress gradients which aid the TO in determining the elements that contribute the least in the optimization problem. The element densities are updated

in the design space before a new iteration is done and the same process is continued until a final convergence is obtained.

2.6.2 Solid Isotropic Material Penalization

Solid Isotropic Material Penalization (SIMP) has been declared the most implemented and developed approach, Ahmad et al., 2021. SIMP uses the power law to eliminate elements with intermediate densities, where "i" is the element number, "ρ_i" is the density of the ith element, "P" is the penalization factor in the range $1 < P <= 3$ and "k_0", "k_i" are the stiffnesses before and after penalization of the ith element:

$$k_i = (\rho_i)^P k_0 \tag{1}$$

This density-based stiffness is then used to compute the compliance "C", which is the sum of strain energy, and is inversely proportional to the stiffness. This gives the general formulation of SIMP for the compliance minimization problem where "L" is the number of elements and "f_i" and "u_i" is the element force and displacement:

$$\text{Minimize } C = \frac{1}{2}\sum_{i=1}^{L} f_i u_i = \frac{1}{2}\sum_{i=1}^{L} f_i^2 (k_i)^{-1} = \frac{1}{2}\sum_{i=1}^{L} f_i^2 ((\rho_i)^P k_0)^{-1} \tag{2}$$

When utilizing multiple load cases the objective function becomes the weighted compliance "W_c" where "W_q" is the weight of a specific load case, "R" is the number of load cases, and "f_q" and "u_q" are the force and displacement vectors:

$$\text{Minimize } W_c = \frac{1}{2}\sum_{i=1}^{R} W_q f_q^T u_q \tag{3}$$

3 Methods

3.1 Literature search

Google Scholar was the primary resource to find relevant literature. Terms such as "additive manufacturing", "CubeSat", "topology optimization" and "space qualified" was used to find papers relevant to this project. Oria and Research Gate was used as well, but not to the same extent. The results were then further filtered by assessing the relevancy based on the title, then based on the abstract. The literature was filtered based on how closely it fulfilled one or more of the search criteria listed below. If the literature was a close match it was read and additional sources were extracted from the bibliography, which were in turn filtered in the same manner.

The search criteria were as follows:

1. Literature covering additive manufacturing as a whole, i.e. literature reviews, books and standards
2. Literature concerning additive manufacturing of CubeSats
3. Literature concerning Design for Additive Manufacturing
4. Literature concerning Topology Optimization, specifically SIMP

3.2 Software tools

The computer-aided engineering program of choice for the HYPSO team is 3DExperience, a software developed by Dassault Systemes. This is an all in one engineering platform that include capabilities in Computer-aided Design (CAD), FEA and much more. This program combines the simulation capabilities of Abacus Tosca with the user friendly interface of Solidworks and CAD capabilities of Catia V5.

In addition to 3DExperience an online image color summarizer was used to analyze the color content of images. The tool can be found here: *Image Color Summarizer - RGB and HSV Image Statistics* 2022

3.3 Workflow

The workflow used to develop the platform is the proposed DfAM methodology described in section 2.4.1 where the structural optimization was decided to be topology optimized. The structural optimization steps can be seen in Figure 8 and are described in greater detail in the following sections.

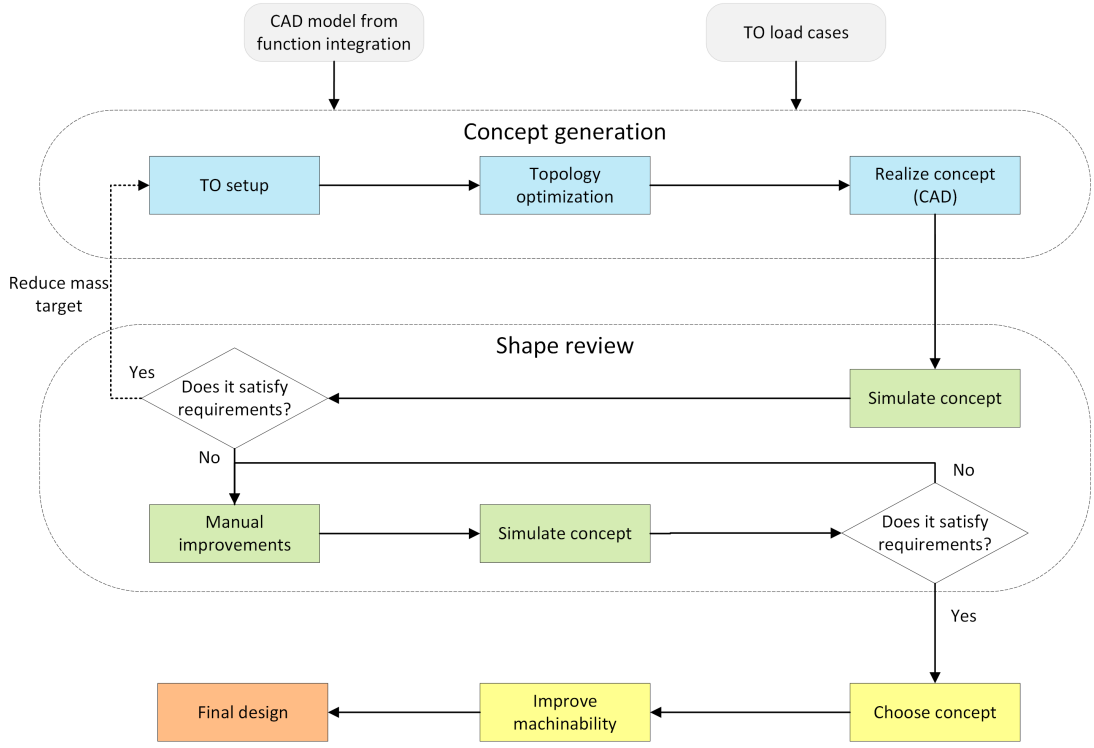

Figure 8: Workflow for structural optimization of the platform

3.4 Function integration

The first step of the process is the function integration, i.e. creating the design space to be optimized. This step was combined with implementing the new components for HYPSO-2, which resulted in some design changes from the HYPSO-1 design. After the parts in the HYPSO-1 design were switched with the new components the function integration began by defining functional surfaces and connecting these with the maximum volume possible to allow the largest design space possible. Then the requirements were reviewed to check whether alterations needed to be done. Assembly requirements were of particular interest due to the significance geometry has towards ease of assembly and need for special tools. Material was therefore removed to enable easy access and

installation of all components. Finally all functional surfaces were partitioned with an appropriate depth so that the functional surfaces could be separated from the design space and can be preserved when doing the TO.

3.5 Concept generation

3.5.1 Choice of strategy

TO support a multitude of constraints and optimization targets. Because of this the user needs to select the most relevant constraints and targets based on the scenario at hand to achieve the best results. In this case the theoretically optimal setup was deemed to be "minimize mass while respecting constraints" as the target with a frequency and stress constraint of 120Hz and 150MPa respectively. This would give the design with the least mass possible while still meeting the requirements for the part. Unfortunately 3DExperience does not support a combination of both frequency and stress constraints so all strategies have to rely on only one. When only one of the constraints were applied the simulation did not converge to any other solution than removing all mass.

As the first strategy did not converge to a usable solution other strategies were attempted. These included combinations of "minimize mass while respecting constraints", "maximize stiffness for a given mass" and "maximize eigenfrequency for a given mass" for the optimization target with a combination of eigenfrequency (120 or 74 Hz), stress (150 MPa) and overhang (>45°) constraints. In the beginning most combinations did not converge to a usable result except for "maximize stiffness for a given mass" with a mass target of 25% or above. This was later discovered to be because of insufficient mesh refinement. Due to having a limitation of 250 000 nodes in total on the educational license it was not possible to test finer meshes until this license was upgraded later in the project. After the license was upgraded several of these combinations were re-tested with improved results when a finer mesh was used.

The strategy that was selected in the end was "maximize stiffness for a given mass" without any constraints and with an overhang constraint of 45°. This was deemed to be the most suitable choice as this strategy converged to the lowest mass target enabling the most weight reduction on the part. Since the strategy has a fixed mass target an iterative approach was used where a lower and lower mass target was set until the simulation either did not converge or the requirements were not met. As a frequency or stress constraint was not applied each iteration was simulated using the loads from the TO to see if the design satisfied the requirements. The iterative approach can be seen in detail in Figure 8.

After the iterative approach was completed without constraints the same was done for the overhang constraint. It was however deemed unnecessary to do all iterations for the overhang constraint as the ease of production does not warrant more than a 50% increase in mass. Therefore the first iteration of the overhang constraint started at the second smallest successful mass target.

3.5.2 Setup

The TO was done using an assembly of all optics, platform and one side of the 6U frame. The optics and 6U frame are contextual parts that are not necessary for the TO and could have been abstracted, but as 3DExperience allows automatic setup of validation simulations based on the TO procedure it was decided to leave them in as this will give more accurate results for the validation simulations that are done after. Including them will also give more accurate results for the frequency simulations in particular as the frame is not particularly stiff and will therefore lower the eigenfrequency significantly.

The assembly was then prepared for simulation by defining the regions to preserve, i.e. the partitioned volumes, and adding connections and restraints. Firstly all bolts were replaced with virtual bolts. Then all contacting surfaces, i.e. the contacts of the HSI train and RGB camera, were tied together to approximate the friction based connections. To get as accurate restraints as possible

the 6U frame was limited in translation normal to each face along the rails in the X-,Y- and Z-direction, mimicking the constraints of the satellite during launch. Lastly the IMU, HSI and RGB sensors w/housing, and star tracker were replaced with a remote mass based on the mass values in Table 2 as these parts did not contribute structurally.

3.5.3 Materials

All parts utilized Al6082-T6, except the platform which used AlSi10Mg. For the platform the material's Z-direction was aligned with the Y-axis, i.e. the intended printing direction (see Section 4.1). The material properties are seen in Table 1.

Table 1: The material properties used, EOS, 2014, *6082-T6 Aluminum* 2022.
*as specified in EOS, 2014

Property	Al6082-T6	AlSi10Mg Heat treated*
Young's Modulus XY $[MPa]$	69000	70000
Young's Modulus Z $[MPa]$	69000	60000
Yield Strength XY $[MPa]$	270	260
Yield Strength Z $[MPa]$	270	250
Density $[g/cm^3]$	2.70	2.67
Poisson's Ration []	0.33	0.33

3.5.4 Loads applied

The TO had 6 load cases based on the force and center of mass of each component on the platform which are seen in Table 2. The force was calculated from the mass of the component by multiplying by $12 \cdot 9.81/1000$ to get the force in Newtons from a 12g load. This was then applied to each corresponding component as a remote force in the center of gravity, but if the component was not included the remote force was applied to the mounting points of the component instead. Three remote forces were created per component, one for each axis. From this the 6 load cases were made by creating two load cases per axis, one in the positive direction and one in the negative direction. This was necessary due to the uncertainty of the load direction during launch.

The initial plan was to use gravity loads, one for each axis, as this is the load the satellite experiences during launch. The reason that remote force was utilized instead of gravity load was due to the TO simulations not converging when gravity loads were used. Remote force applied at the center of gravity of each components was therefore deemed to be the closest approximation of a gravity load. For the same reason the pre-tightening of the virtual bolts were removed.

3.5.5 Meshing

Initially the mesh used the suggested element size with a size of 4.76mm for the mount and 6.47mm for the 6U frame, with the rest being equal to the values in Table 3. This gave a total of 186 918 elements. A mesh size of 4mm was used on the frame to get at least two layers of elements. This was done to better capture bending and moments as this is not properly captured in first order elements with a single layer. Then an iterative approach was used to check the smallest mesh size that could be used successfully. A size of 1.4mm for the mount was used in the end which resulted in a total of 4 684 264 elements. Further mesh refinement was attempted, but this lead to the simulation failing. 1.4mm was therefore deemed sufficient for the TO as the TO converged at this size for all mass targets.

Table 2: The mass, force applied and center of mass for each component on the platform

Component	Mass [g]	12G force [N]	Center of Mass [mm]
IMU	55.0	6.47	(-33.1, -29.9, -11.8)
Star Tracker	155.0	18.25	(52.2, -6.6, 106.4)
HSI Detector + house	140.6	16.55	(16.3, -0.8, -59.6)
RGB detector + house	143.0	16.83	(-50.8, -0.2, 84.5)
Grating + cassette	52.7	6.20	(-3.3, 2.1, 27.1)
RGB objective	106.0	12.48	(-51, 0, 145.1)
HSI front lens	104.0	12.24	(0, 0, 137.8)
HSI mid lens	104.0	12.24	(0, 0, 63.3)
HSI rear lens	104.0	12.24	(6.2, 0, -4.6)
Slit tube	46.0	5.42	(0, 0, 100.4)

Table 3: The element sizes, number of elements and percent of good quality elements of the mesh

Part	Mesh size	Elements	Good elements [%]
Mount	1.4mm	4,618,798	99.99 %
HSI front lens	3.74mm	3,017	99.97 %
HSI mid lens	3.74mm	2,913	99.83 %
HSI rear lens	3.74mm	3,024	97.52 %
Slit tube	3.14mm	6,190	99.34 %
RGB lens	4.25mm	7,272	91.96 %
HSI brackets (x4)	1.79mm	10,660	100.00 %
RGB brackets (x2)	1.67mm	5,009	100.00 %
6U frame	4mm	27,333	98.65 %
Total		4,684,264	99.97 %

3.6 Shape review

3.6.1 Concept simulation

After the TO was done the concept was simulated to verify that the structural integrity was sufficient to satisfy the requirements. The stress and the first 5 modes of the eigenfrequency of each concept were simulated to verify the structural integrity of each concept.

The simulations used the "validate concept" function in 3DExperience where simulations could be automatically set up using the generated concept form the TO. This automatically set up simulation was identical to the TO and would therefore require some minor edits to set up the simulation for a specific concept. Specifically it was necessary to edit the number of virtual bolt connections as the TO had removed several of the mounting points for the bolts.

In addition to the concept-by-concept edit of virtual bolts, the validation simulations all switched the load cases from remote force to gravity to account for the mass of the optimized part. The pre-tightening load of 96N was also included on all bolts for the HSI and RGB camera to account for the stresses these apply. A frequency step for the first 5 modes was added as well to get the eigenfrequency of each concept.

3.6.2 Manual changes

The last step of the structural optimization process was implementing manual changes to the concepts if they did not satisfy the requirements. The changes to the concepts were mainly adding material in certain places to account for the missing pre-tightening on the virtual bolts or to improve the eigenfrequency or displacement. After the manual changes were implemented the concept was simulated again to verify that the concept now satisfied the requirements.

Finally, after a final concept was selected, manual changes were implemented to improve the machinability of the concept. This was mainly done by either adding fastening points to hold the part while machining or by slightly moving the geometry to one side to create more room for a machining tool. The design was then simulated again to verify that it still met the requirements.

3.6.3 Overhang analysis

To compare the amount of overhang between concepts the built in overhang analysis tool was used from 3DExperience. This tool adds either a yellow color to angles below 45° from horizontal or red color to areas that are horizontal. As this tool does not quantify the colored areas a color analysis was done on images taken of the colored models. To get images that can be compared the images were taken with the same view in 3DExperience and were then cropped to 600x800 pixels. This ensures that the concepts are equally sized. Then an image color summarizer was used that separated the colors into 4 groups, black, grey, red and yellow which then were given a percentage based on the amount of pixels each color had in the image.

4 Function integration

The first step when creating the new design was to replace the parts that had been updated, which were the RGB camera and star tracker. As the dimensions of these parts differed somewhat to the original parts and the mounting solution for the new star tracker was in a new position, this meant that the current design needed to be adjusted somewhat to accommodate the new parts.

After the new parts were accommodated the next step was to begin the function integration process. This started by mapping the functional surfaces, which can be seen in Figure 9. Then these surfaces were connected with a functional volume to create the design space for the part. This volume was maximized to allow the widest range of possible solutions from the TO as possible. After this step it was apparent that the placement of the IMU was not ideal as it would be very close the the RGB camera. It was therefore decided to move this to a more advantageous placement closer to the rear, which would reduce the cable length necessary for the IMU cable.

4.1 Assembly and manufacturing requirements

After the design space was created the assembly and manufacturing requirements were accounted for. To ease manufacturing it was decided to design for a +Y print direction. This would reduce the time needed for manufacturing as the part would be much shorter than a X-, or Z-axis print, and would therefore require less layers, reducing the printing time and cost.

To accommodate this printing direction the assembly was designed in such a way that most parts were inserted from the top, i.e. in the -Y direction. This would eliminate support for overhang above these parts as the material would be removed to make room for the assembly process. The exceptions to this are the star tracker and lenses. These were excluded from this assembly direction due to the length of the components. It was therefore deemed more beneficial to allow material above these components and mount them from the side instead as the removal of all material above these components would significantly reduce the design space and therefore potentially reduce the stiffness of the part.

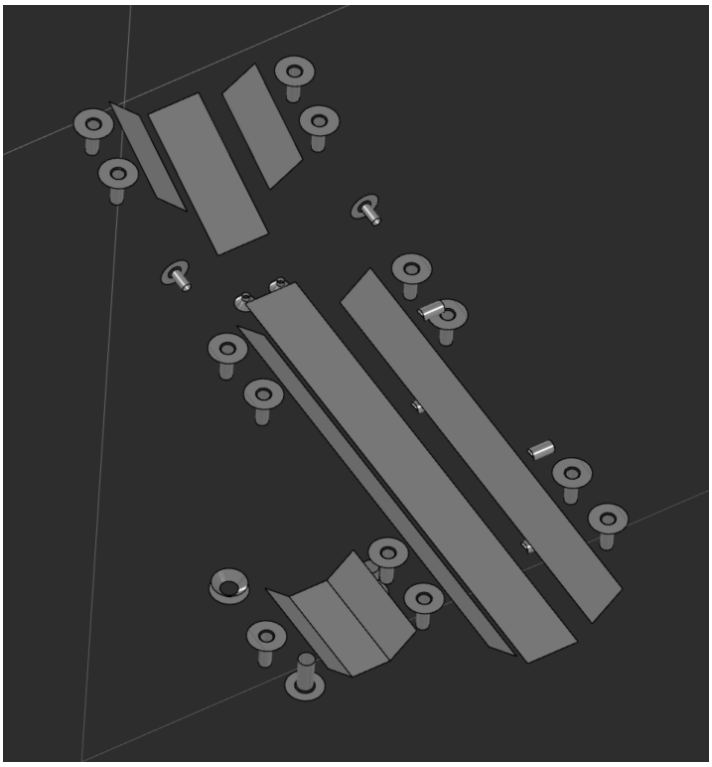

Figure 9: The functional surfaces extracted

The rotation of the countersunk holes on the grating cassette was a part of this assembly decision. By rotating the holes 90° the holes face in the +Y direction instead, ensuring that they are accessible for assembly. The countersunk holes were also offset by 0.1mm in the -X and +Z direction so that the cassette would be pressed towards a corner, ensuring the cassette is correctly placed.

Other changes that were implemented include room for cables and preparation for machining. In particular it was important to account for the new and larger cables for the RGB camera. A cutout was therefore made to make sure the cables could be routed without colliding with the mount. In regards to preparing for machining it was decided to add an extra 0.4mm of material on leading edges for the HSI train and RGB camera. This was to ensure that there was enough material to machine a flat surface with the proper dimensions. Machining these surfaces was deemed necessary due to the uncertainty in the correctness of the geometry after printing. It is crucial that the HSI train is aligned properly and therefore machining was deemed necessary on the leading surfaces of the HSI train.

Another design change was the addition of alignment holes for the HSI and RGB sensor. This feature is the addition of 2 holes for bolts per sensor that fasten the sensor housings directly to the mount. This therefore removes the need for manual alignment of the sensors. This is particularly useful for the HSI sensor as it is crucial that this is parallel to the grating and previously required manual calibration while assembling to ensure that it was rotated correctly. This addition should therefore reduce the assembly time by removing the need for calibration. The hole faces are machined after printing to ensure that they are parallel to the grating.

Finally, material was added to provide mounting points to the frame where it was suitable. This was decided to be on the +Y side as this would allow a stable base on the bottom with upwards reaching mounting points, thus reducing the amount of support needed as opposed to having it on the -Y side. For the rear most mounting an overhang angle of 60° was used to remove the need for supports. The resulting design space can be seen in Figure 10.

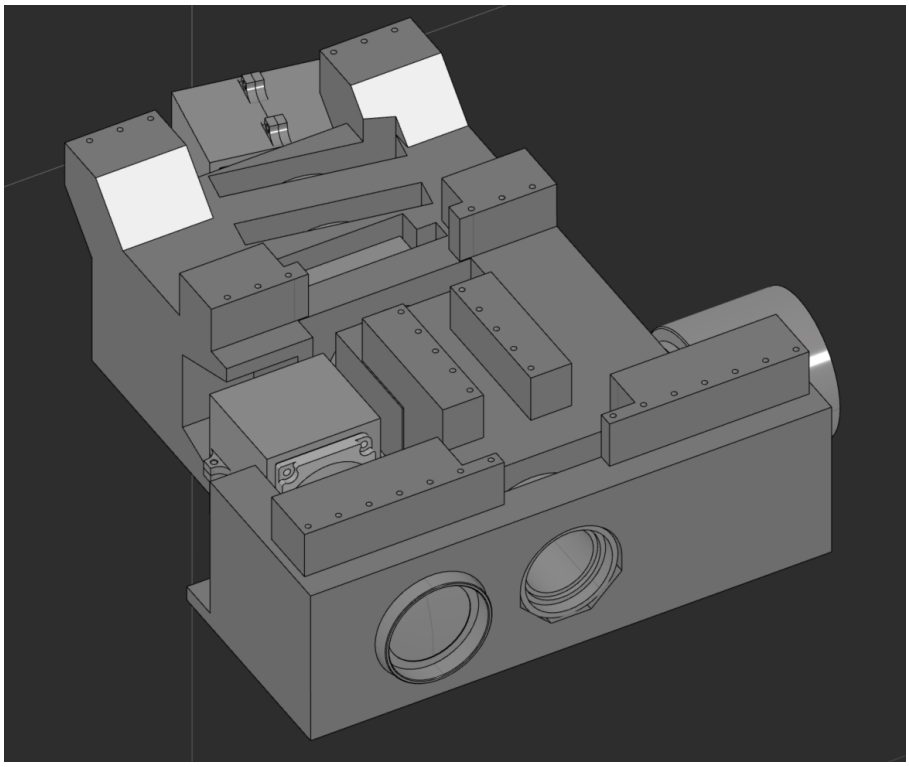

Figure 10: The resulting design space

4.2 Partitioning

The final step of function integration was partitioning out faces to keep. This was primarily the functional surfaces from the first step with some modifications. The first modification was the reduction of the HSI train v-groove. It was deemed unnecessary to keep the whole groove, and only the part directly beneath the mounting brackets were kept as these areas were necessary to fasten the optics. Parts of the contacting faces for the grating cassette was also kept to ensure the cassette had faces to use for alignment.

Otherwise all flat faces, i.e. v-groove and cassette contacting faces, were partitioned with a depth of 4mm and all mounting holes except those for the 6U frame were partitioned with a thickness of 2mm. The holes for the 6U frame were not included in the partitioning so that the TO could freely select what holes were necessary.

5 Results

5.1 Generated designs

The first TO simulation was without any constraints and used a mass target of 25% (841g) from the original weight of 3366g. This was followed up by mass targets of 15% (505g), 10% (337g), 7.5% (252g) and finally 5% (168g). As the 5% mass target did not satisfy the requirements no further reduction was attempted. After this the overhang constraint simulations were done. This used a mass target of 7.5% and 5%. 5% did not satisfy requirements with an overhang constraint either, and was therefore the last mass target attempted. The generated concepts can be seen in Figure 11.

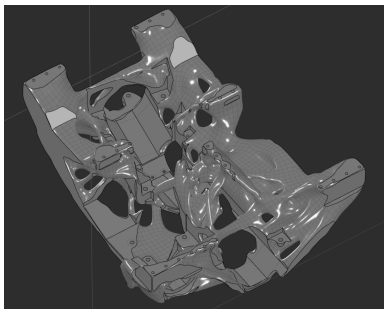

(a) 25% mass

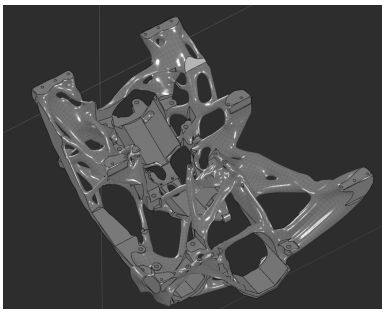

(b) 15% mass

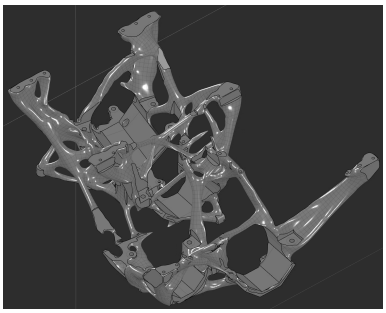

(c) 10% mass

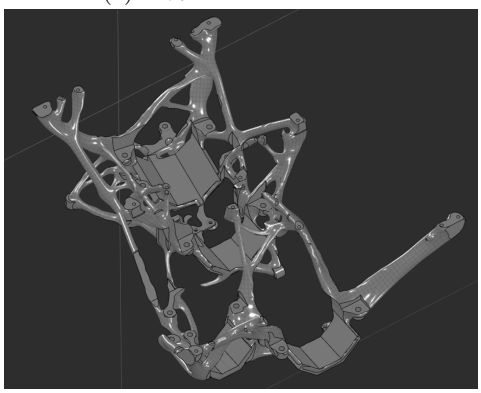

(d) 7.5% mass

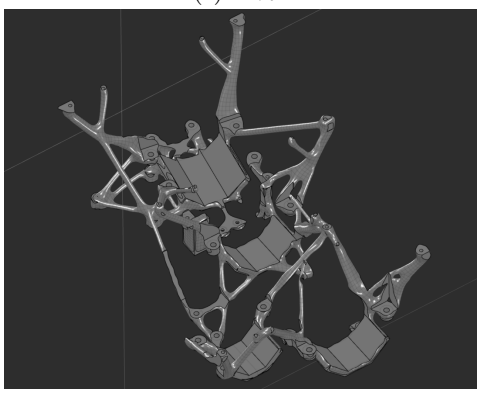

(e) 5% mass

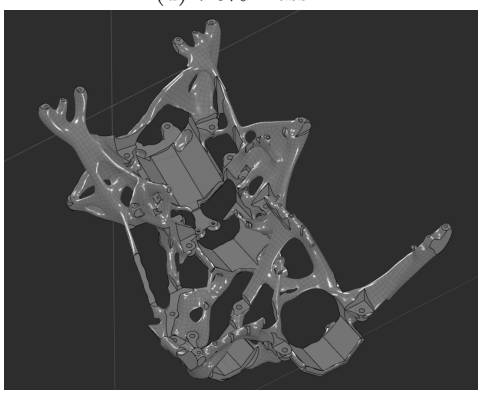

(f) 7.5% mass with overhang constraint

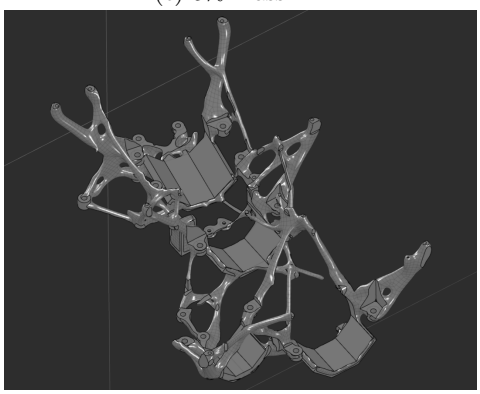

(g) 5% mass with overhang constraint

Figure 11: The generated concepts from the TO

5.2 Simulation results

The eigenfrequency, stress and displacement can be seen in Figure 12, 13 and 14 respectively. In the included table it can be seen that the 5% concept does not satisfy the stress requirement of max 150 MPa in the +X direction as the stress was simulated to be 388 MPa, which is why no further reduction was attempted. The same can be seen for the 5% with overhang constraint for all directions where the stress is between 3540 - 12500 MPa, well above the limit of 150 MPa.

The field plots given by the validation simulations, specifically the frequency mode plots and displacement plots, are later used as a basis for manual improvement of the design of the 5% and 5% with overhang constraint concepts. These can therefore be seen below in Figure 15 and 16 without the overhang constraint and in Figure 17 and 18 with the overhang constraint.

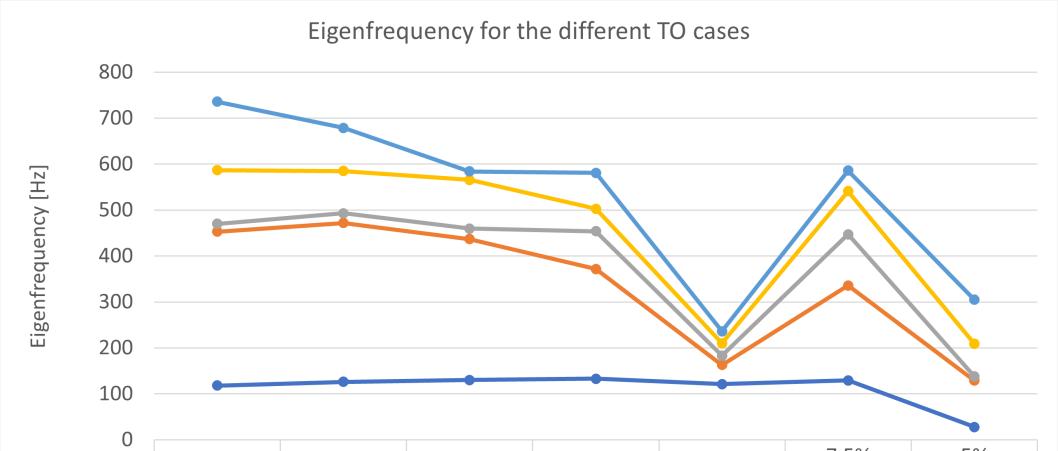

	25 %	15 %	10 %	7.5 %	5 %	7.5% Overhang	5% Overhang
Mode 1	118	126	130	133	121	129	28
Mode 2	453	472	437	372	163	336	129
Mode 3	470	493	460	454	183	447	138
Mode 4	587	585	566	503	210	541	209
Mode 5	736	679	584	581	236	586	305

Figure 12: The eigenfrequencies of the different generated concepts

5.3 Manual changes

5.3.1 5% concept

Figure 15 and 16 were used as the basis for the manual changes for the 5% concept. From these figures it is evident that the mounting holes for the grating cassette on the under side of the platform are not sufficiently supported as all 5 eigenfrequency modes in Figure 16 are based on the lack of stiffness in this area. This is also seen in the displacement plots in Figure 15, in particular subplot (b),(c) and (d). This was remedied by adding material to adjacent parts on the platform, significantly increasing the stiffness of this area.

From subplot (a) in Figure 15 it can be seen that the RGB has a large displacement. Closer inspection showed that this was due to a lack of support under the front RGB bracket which meant that the RGB was only supported on one side. To remedy this additional material was added between the front RGB bracket mounting holes and the v-groove. To ensure an efficient force path on all brackets the same was done on the remaining bracket mounting holes that did not have material that went straight from the mounting hole to the v-groove below. This manual change was likely necessary due to the pre-tightening on the bolts not being accounted for in the TO.

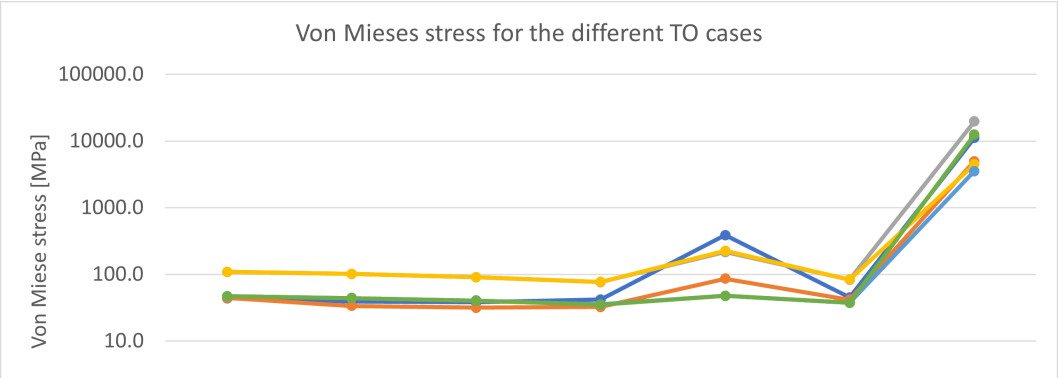

	25 %	15 %	10 %	7.5 %	5 %	7.5% Overhang	5% Overhang
+X	43.9	39.0	38.0	41.9	388	45.3	11100
-X	44.4	33.7	31.6	32.3	86.2	41.7	4980
+Y	109	101	90.7	76.7	216	83.5	19700
-Y	109	101	91.0	77.0	225	83.8	4460
+Z	47.1	44.1	40.5	35.4	47.6	37.7	3540
-Z	46.8	44.1	40.2	35.1	47.5	37.4	12500

Figure 13: The Von Mieses stress of the different generated concepts

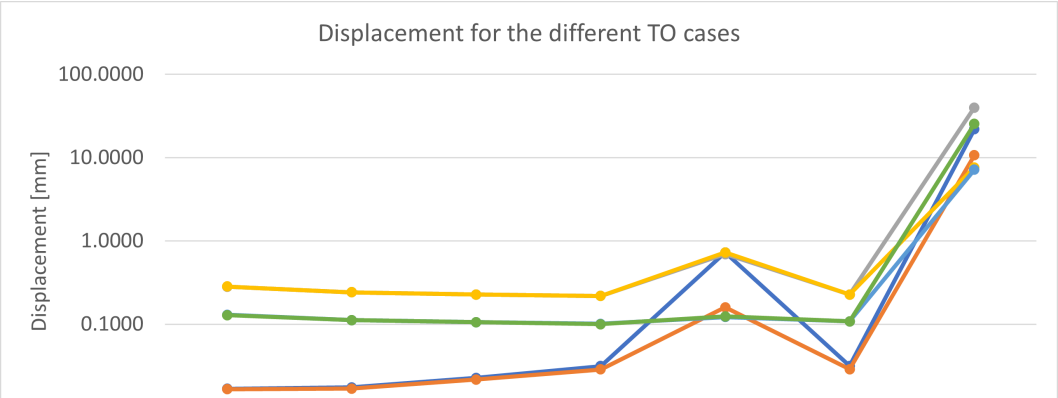

	25 %	15 %	10 %	7.5 %	5 %	7.5% Overhang	5% Overhang
+X	0.0168	0.0175	0.0227	0.0314	0.729	0.0316	21.9
-X	0.0166	0.0169	0.0217	0.0287	0.160	0.0289	10.7
+Y	0.283	0.242	0.227	0.219	0.695	0.227	39.9
-Y	0.284	0.242	0.227	0.219	0.728	0.228	7.64
+Z	0.130	0.112	0.106	0.101	0.122	0.108	7.16
-Z	0.129	0.112	0.106	0.100	0.124	0.108	25.5

Figure 14: The displacement of the different generated concepts

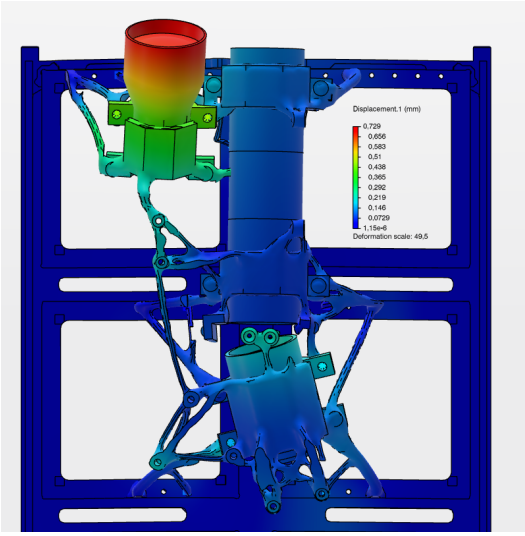

(a) +X

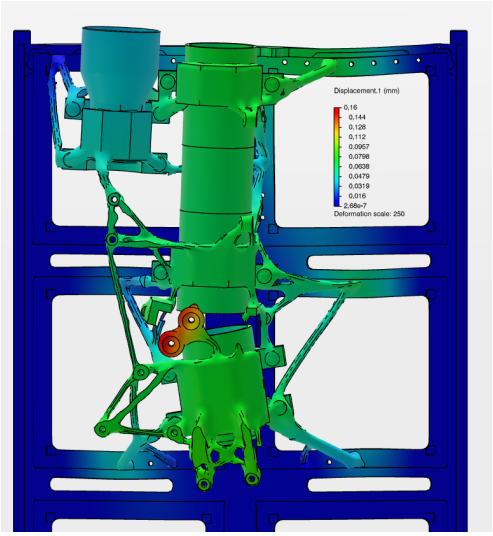

(b) -X

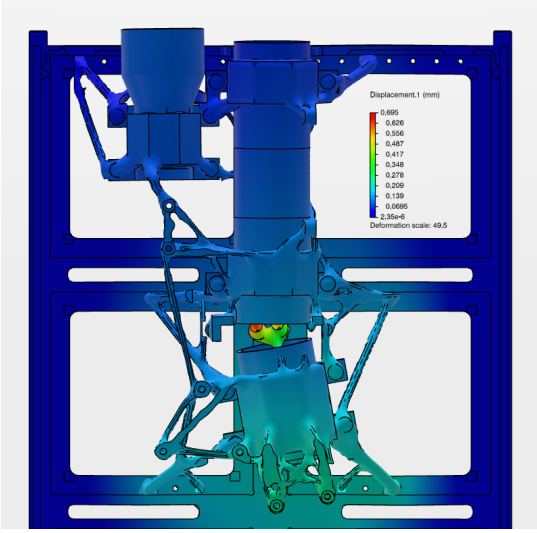

(c) +Y

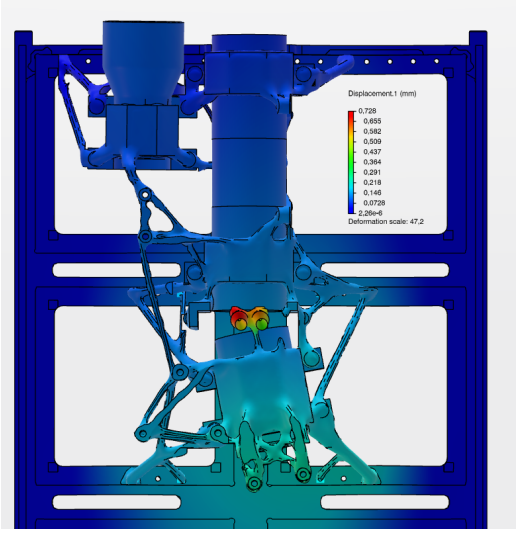

(d) -Y

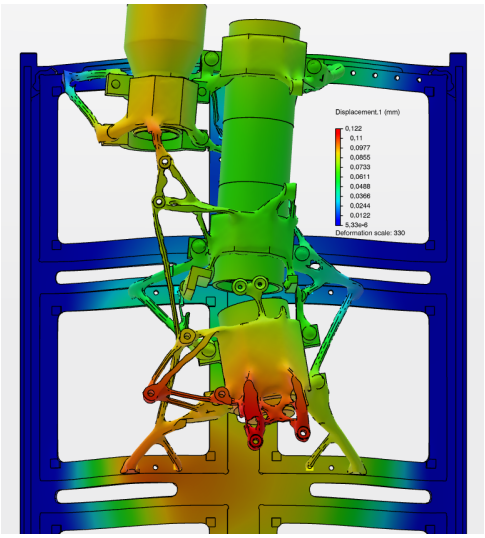

(e) +Z

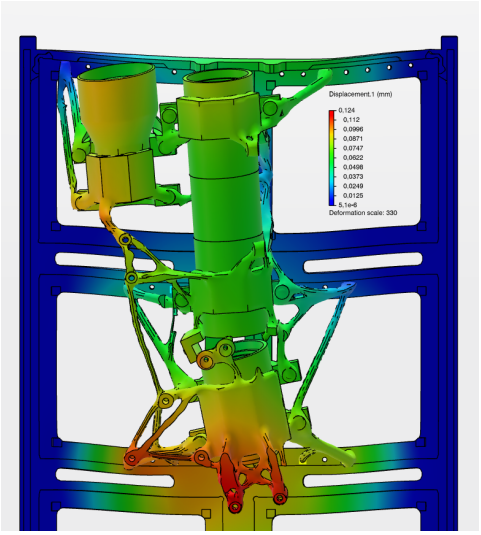

(f) -Z

Figure 15: The displacement for the 5% concept

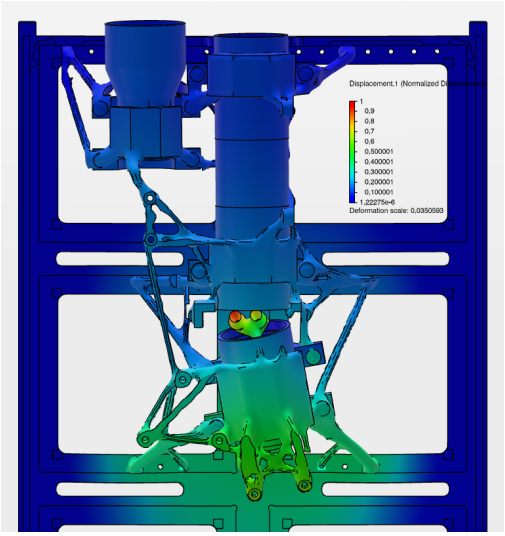

(a) Mode 1

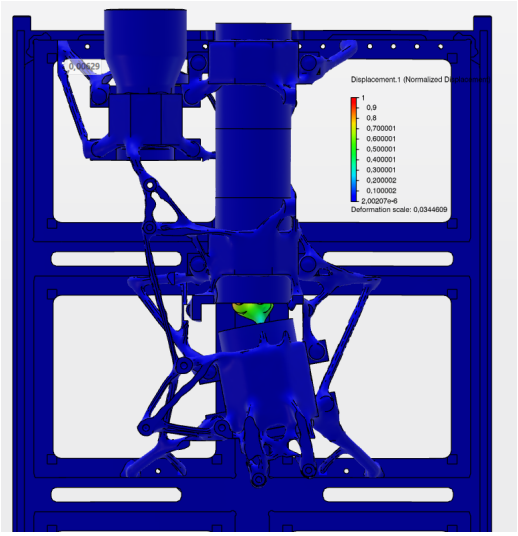

(b) Mode 2

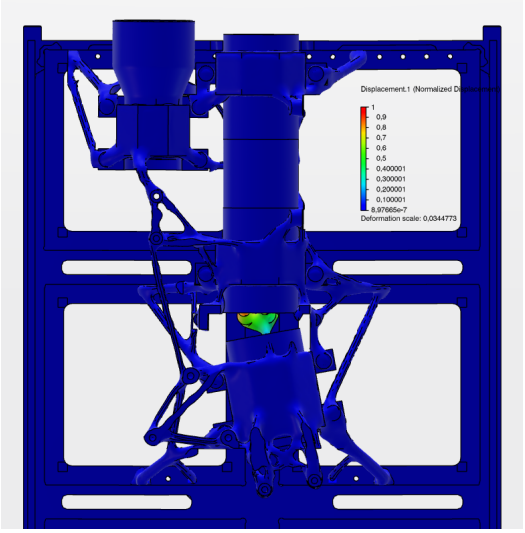

(c) Mode 3

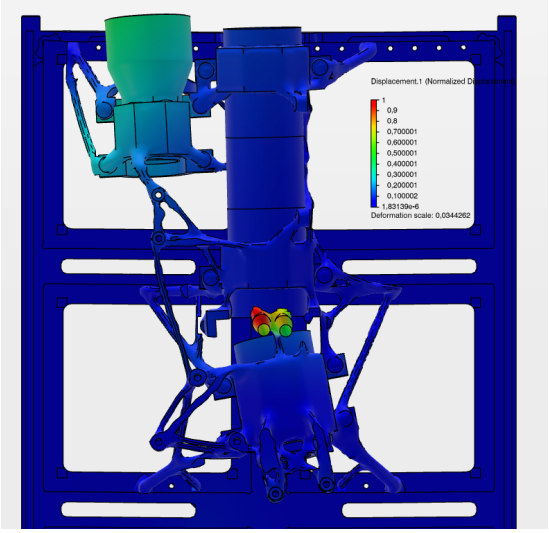

(d) Mode 4

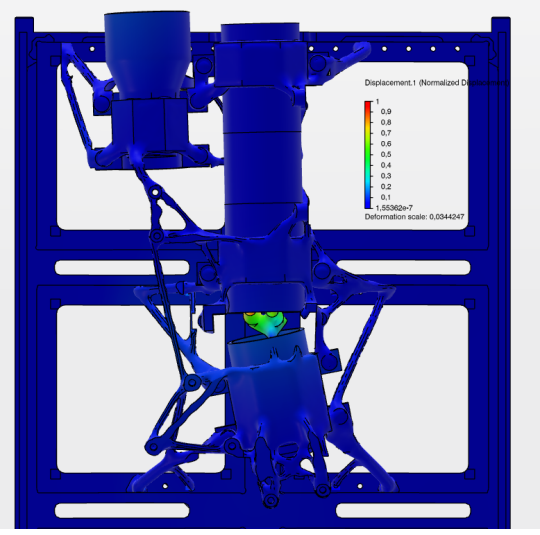

(e) Mode 5

Figure 16: The frequency modes for the 5% concept

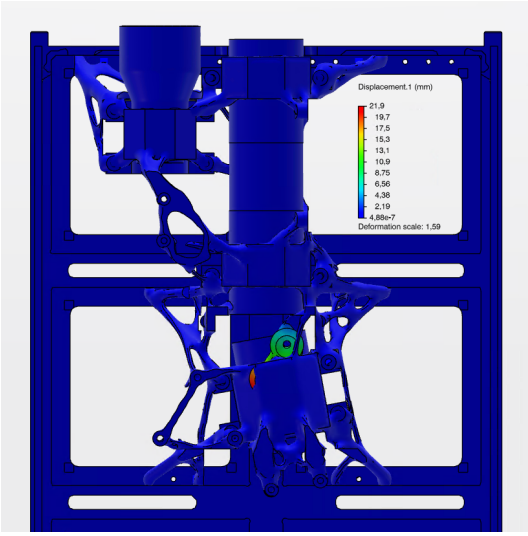

(a) +X

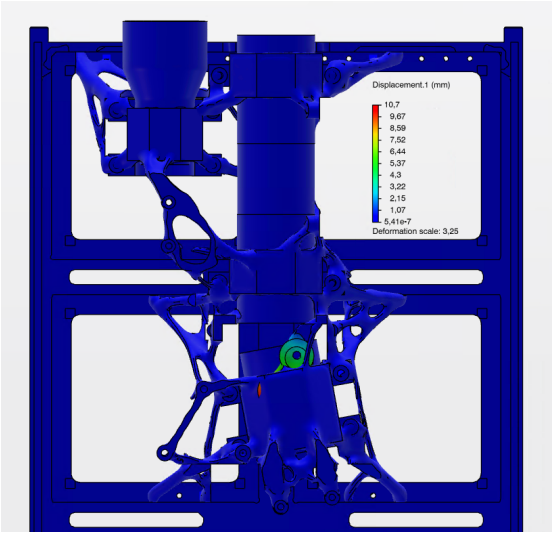

(b) -X

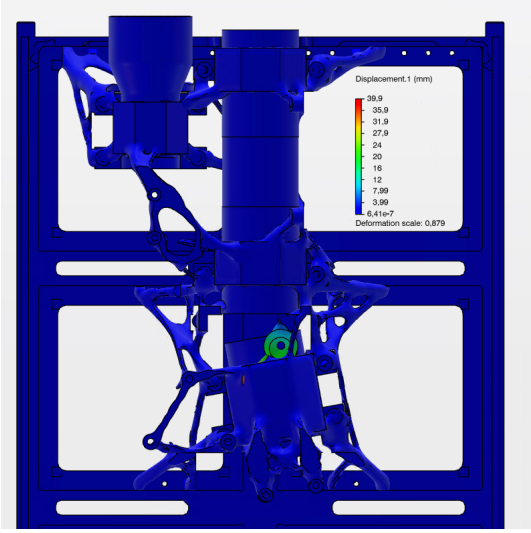

(c) +Y

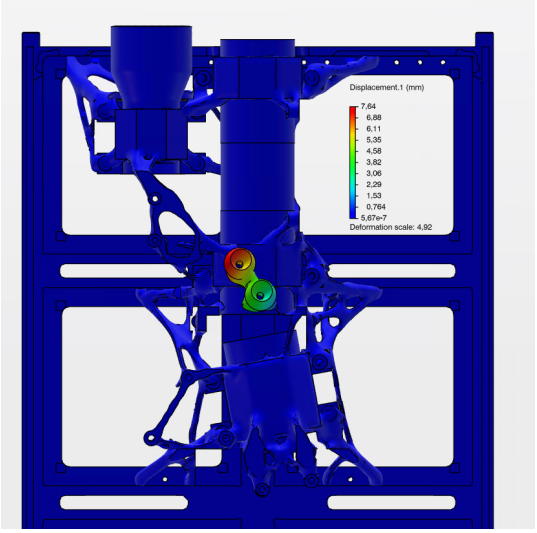

(d) -Y

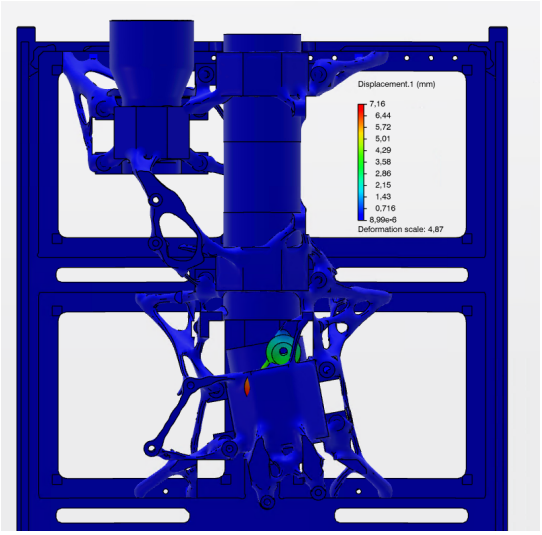

(e) +Z

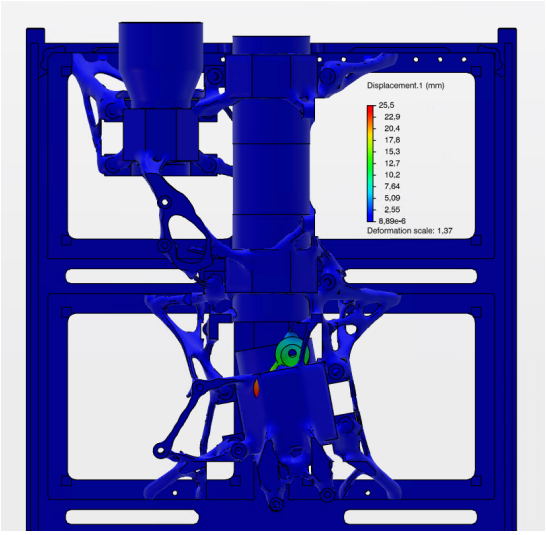

(f) -Z

Figure 17: The displacement for the 5% with overhang constraint concept

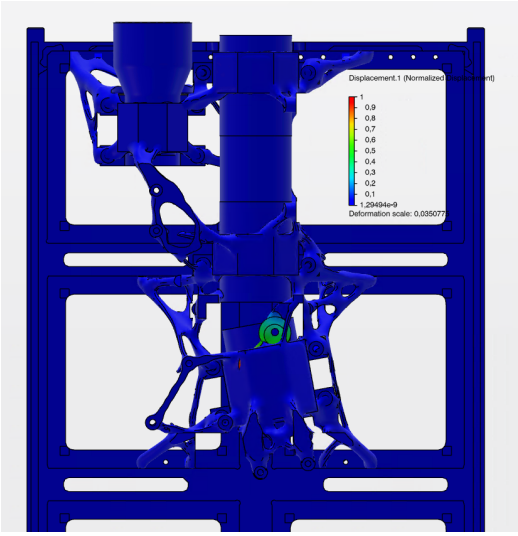

(a) Mode 1

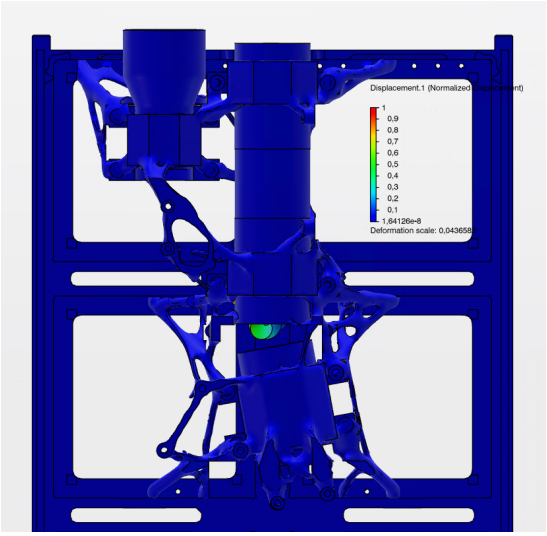

(b) Mode 2

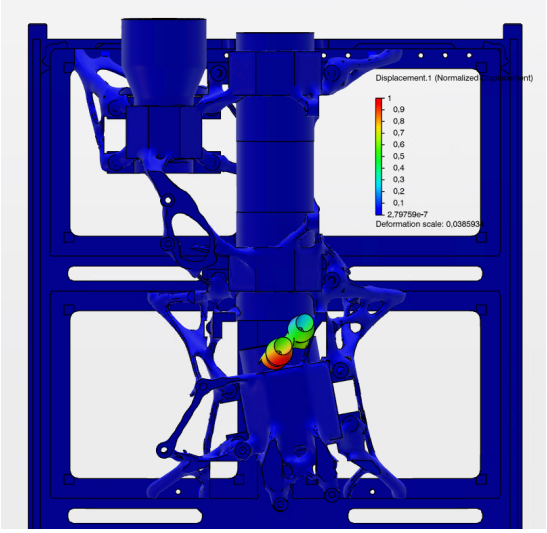

(c) Mode 3

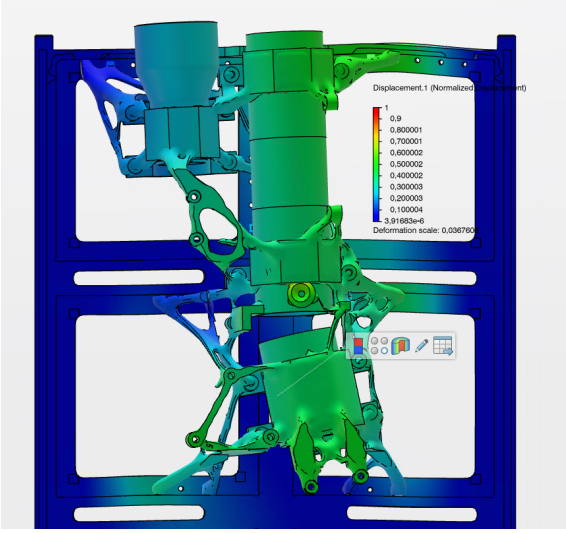

(d) Mode 4

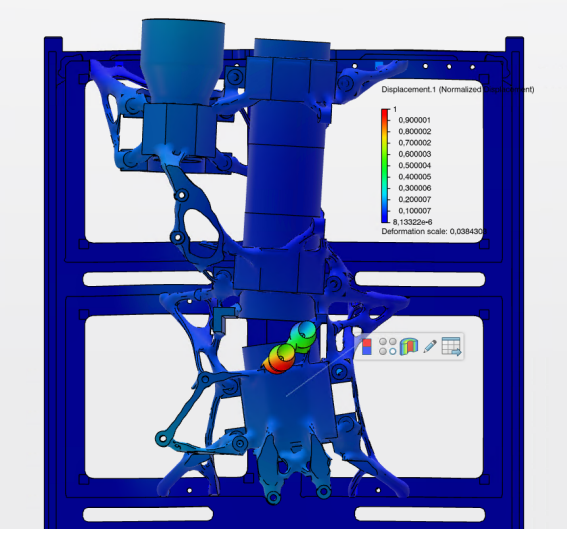

(e) Mode 5

Figure 18: The frequency modes for the 5% with overhang constraint concept

Lastly some superfluous material was removed. This was mainly artifacts from the TO, such as spikes that did not connect any areas or material that lead up to a mounting point on the 6U frame that were deemed to not significantly contribute to the stiffness of the part. All changes are shown in Figure 19 and are marked with red for removal of material and with green for added material.

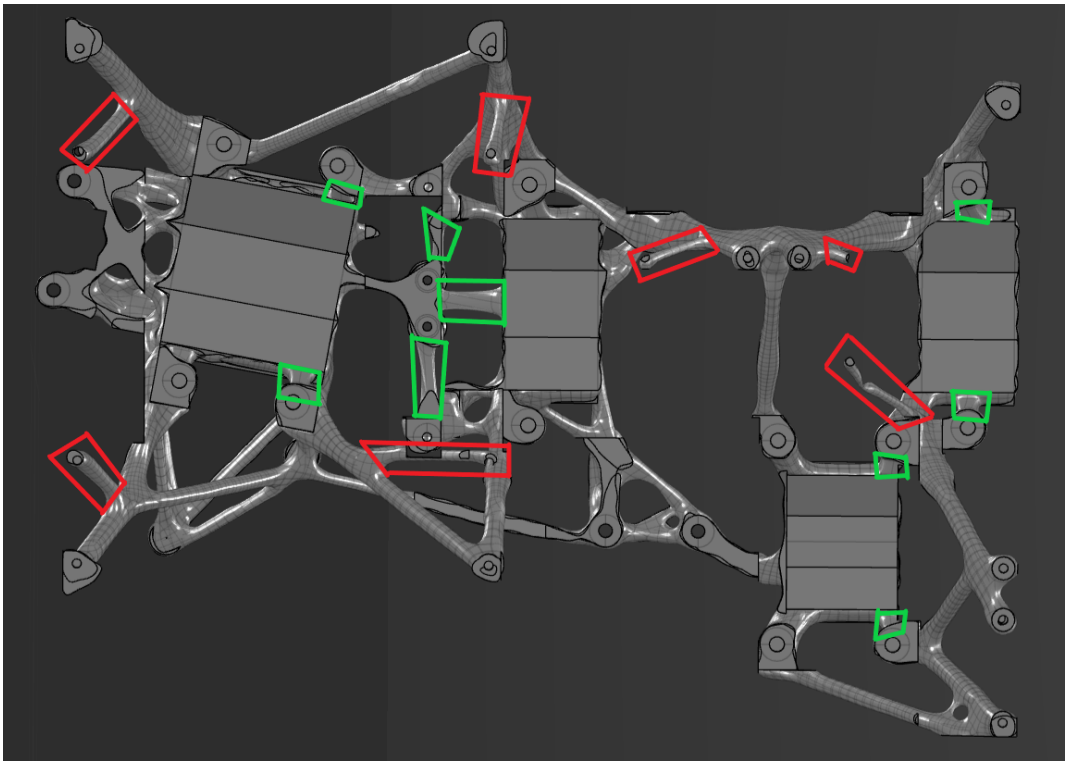

Figure 19: The manual changes to the 5% concept with added material in green and removed material in red

5.3.2 5% with overhang constraint concept

Similarly to the previous concept Figure 17 and 18 were used to identify improvements. The 5% with overhang constraint concept has the same issues as the 5% concept without the overhang constraint except for the missing support for the RGB camera. Therefore the same manual changes were implemented here as well wherever necessary. All changes are shown in Figure 20 and are marked with red for removal of material and with green for added material.

5.4 Comparison between edited and unedited parts

In Figure 21, 22 and 23 the eigenfrequency, displacement and stress from the edited and unedited versions of the 5% concepts can be seen. From these figures it can be seen that the manual changes has greatly improved the measured metrics significantly, especially for the 5% overhang version. This version has improved the eigenfrequency from 28 Hz to 133 Hz, the displacement from a max of 39.9 mm to 0.212 mm and the stress from a max of 12500 MPa to 87.2 MPa. Both edited parts pass the requirements as they have a minimum eigenfrequency above 74 Hz and a maximum stress in all directions below 150 MPa. The maximum displacement is also significantly reduced, reducing the likelihood of interfering with other parts.

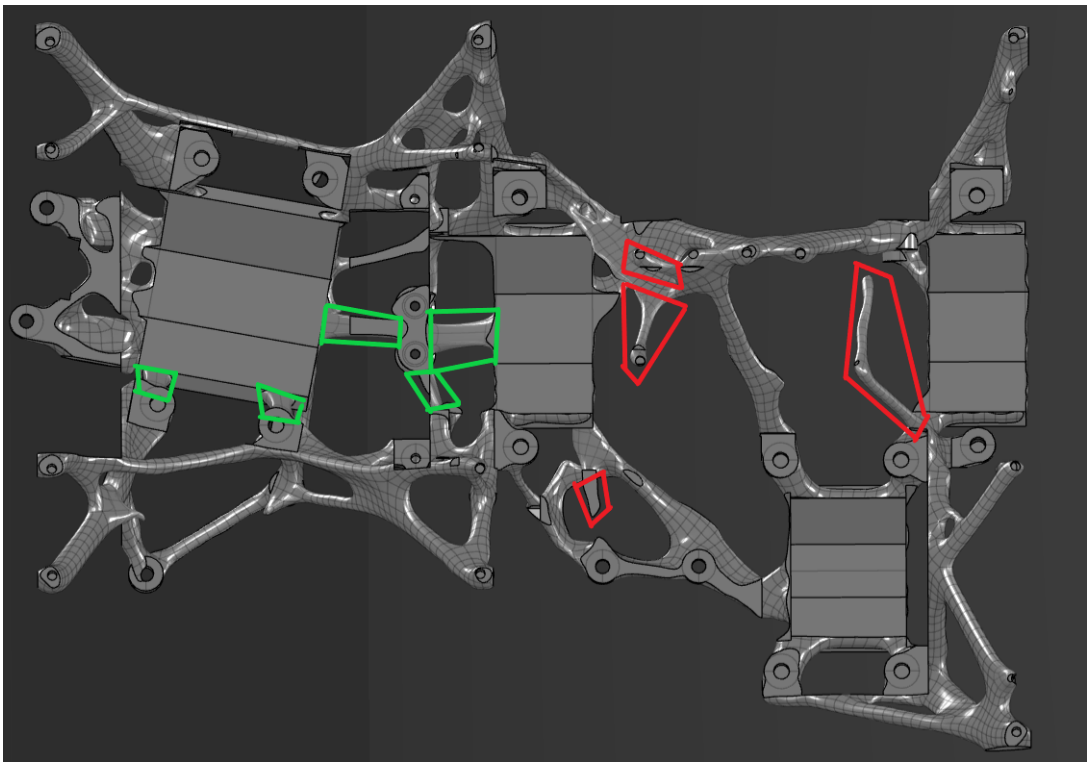

Figure 20: The manual changes to the 5% with overhang constraint concept with added material in green and removed material in red

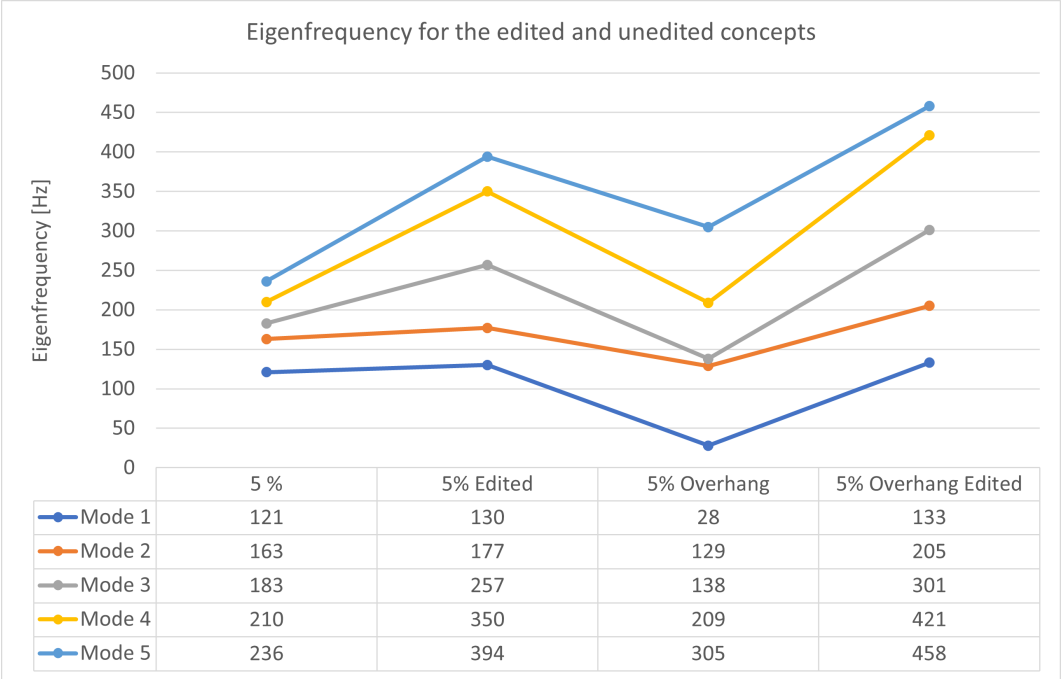

	5 %	5% Edited	5% Overhang	5% Overhang Edited
Mode 1	121	130	28	133
Mode 2	163	177	129	205
Mode 3	183	257	138	301
Mode 4	210	350	209	421
Mode 5	236	394	305	458

Figure 21: The eigenfrequencies of the edited and unedited 5% concepts

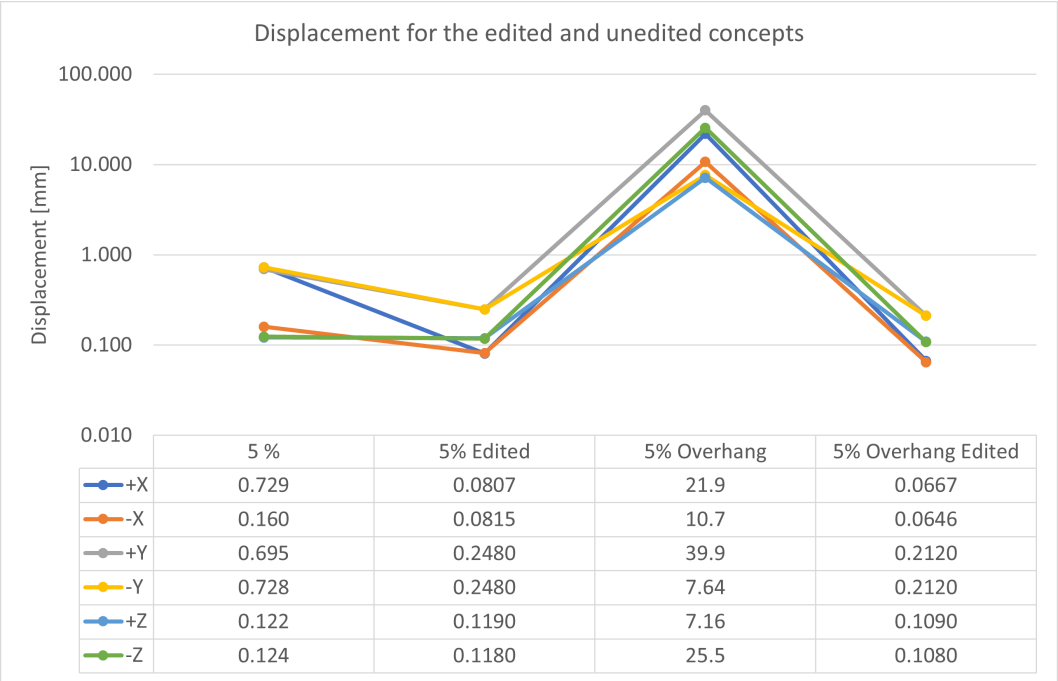

	5 %	5% Edited	5% Overhang	5% Overhang Edited
+X	0.729	0.0807	21.9	0.0667
-X	0.160	0.0815	10.7	0.0646
+Y	0.695	0.2480	39.9	0.2120
-Y	0.728	0.2480	7.64	0.2120
+Z	0.122	0.1190	7.16	0.1090
-Z	0.124	0.1180	25.5	0.1080

Figure 22: The displacements of the edited and unedited 5% concepts

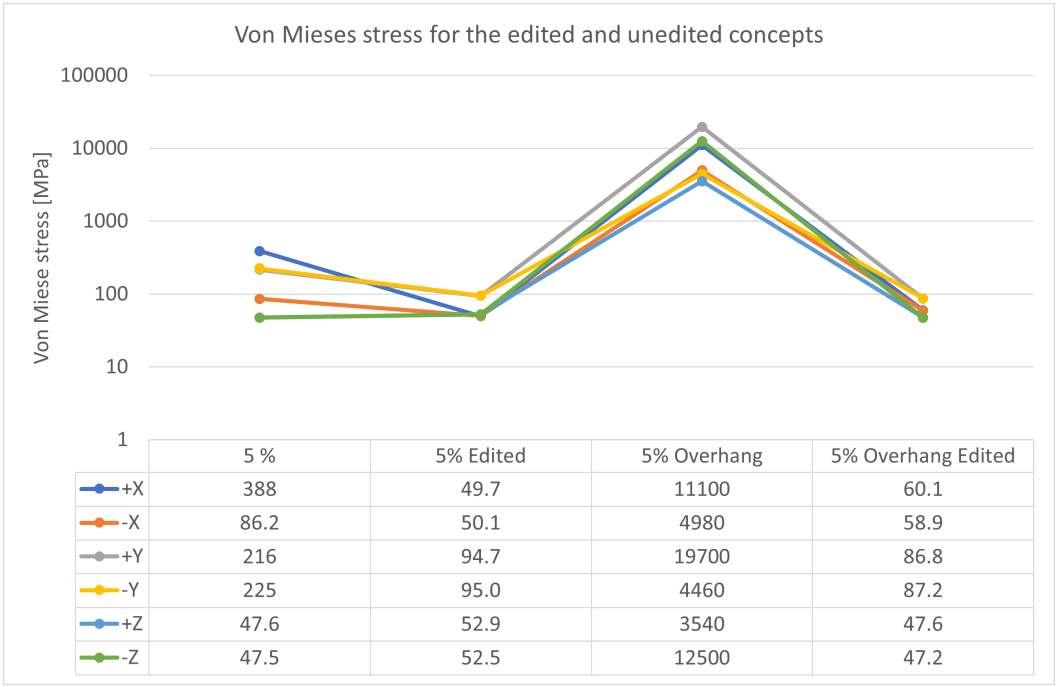

	5 %	5% Edited	5% Overhang	5% Overhang Edited
+X	388	49.7	11100	60.1
-X	86.2	50.1	4980	58.9
+Y	216	94.7	19700	86.8
-Y	225	95.0	4460	87.2
+Z	47.6	52.9	3540	47.6
-Z	47.5	52.5	12500	47.2

Figure 23: The stresses of the edited and unedited 5% concepts

5.5 Choice of concept

When choosing the final concept the mass, eigenfrequency, stress, displacement and overhang angle were looked at to determine which of the two concepts would be the most suitable. A comparison between the eigenfrequency, stress and displacement was made, which showed that the 5% overhang concept had a slight edge in all three measures. The concepts varied the most when it came to max displacement, where the max displacement was 0.248mm vs 0.212mm for the 5% and 5% overhang respectively.

Next was the mass, where the 5% concept and 5% overhang concept had a mass of 156g and 180g respectively. This meant that the two concept was practically equally suitable, as the 5% concept was a little lighter, but with comparatively worse eigenfrequency, stress and displacement.

The last factor to be considered was the amount of support necessary, i.e. the overhang angle of the part. Figure 24 shows the amount of overhang for both concepts. The colors of these images were analyzed to find the area with horizontal and <45° overhang angles and the ratio of colors can be seen in Table 4. From the table it can be seen that the 5% concept has 6.75% yellow pixels to the 4.44% for the 5% overhang concept. This represents a 52% increase in support needed.

As the two concepts are fairly equal in terms of weight and strength, it was deemed that the reduced support usage in combination with slightly better eigenfrequency, stress and displacement values outweighed the detriment of a slightly increased mass. The 5% with overhang constraint was therefore selected as the final concept to prepare for manufacturing.

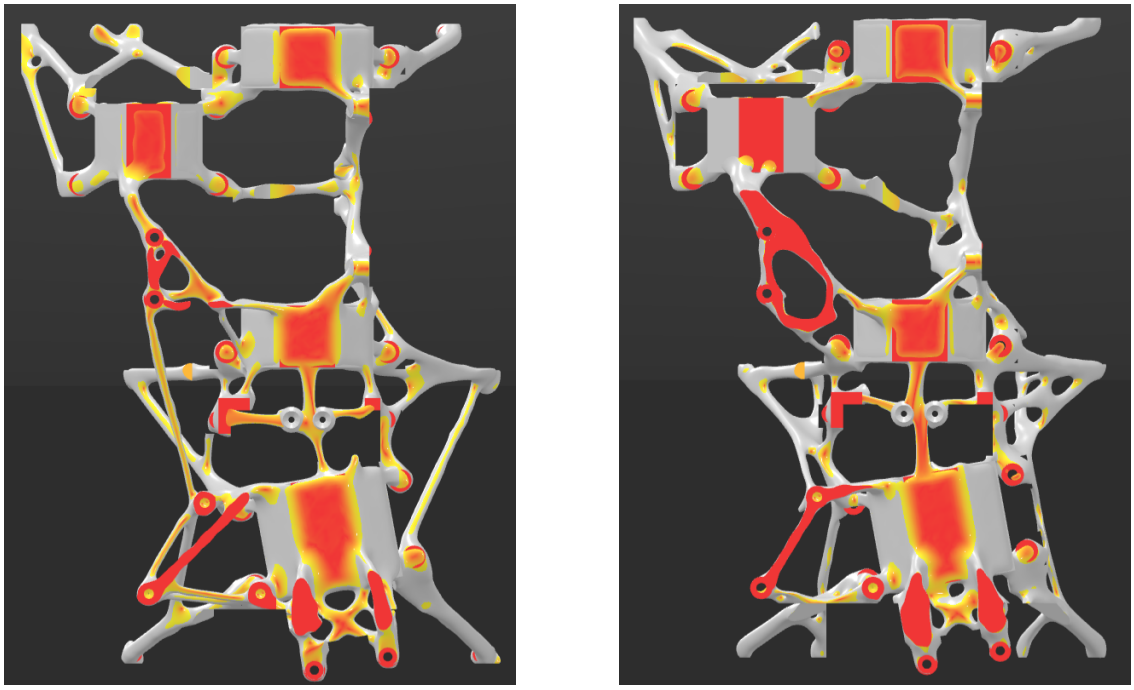

(a) 5% concept

(b) 5% with overhang constraint concept

Figure 24: The amount of overhang above 45°(yellow) and horizontal(red) for the two concepts

Concept	Black	Grey	Red	Yellow
5% Edited	70.53%	15.87%	7.03%	6.75%
5% Edited Overhang	69.00%	18.56%	7.99%	4.44%

Table 4: The color composition of Figure 24

5.6 Preparation for manufacturing

To prepare the part for manufacturing two modifications were done. The first modification was making the 6U frame mounting holes sufficiently thick. Since the area around the holes were not set to be preserved in the TO this was necessary to ensure sufficient thickness for the threads. To ease manufacturing an angle of 60° was placed underneath the overhang of the added material. An example can be seen in Figure 25.

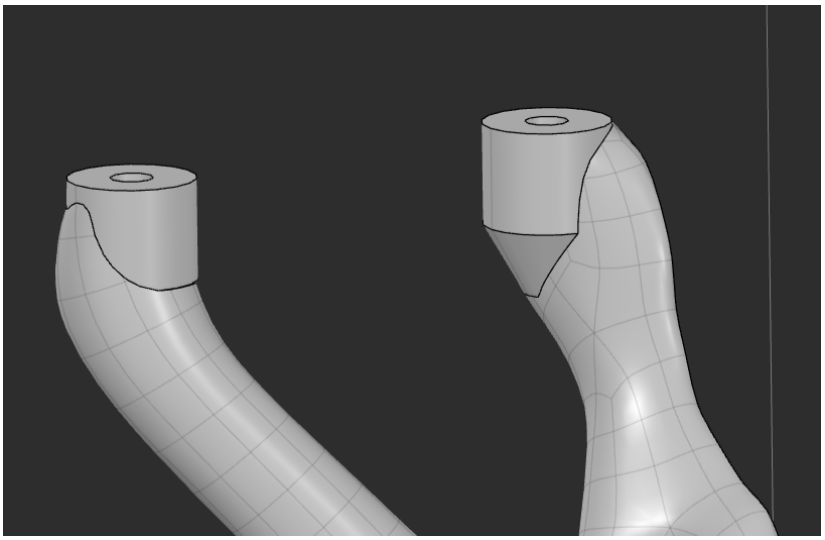

Figure 25: The reinforced mounting points with a 60° overhang angle

The second change was the addition of fastening points for the machining that needs to be done to ensure correct tolerances. Four fastening points were therefore added in areas that were easy to reach and close to the faces to be machined to ensure that the fastening points were effective. The four points added can be seen in Figure 26.

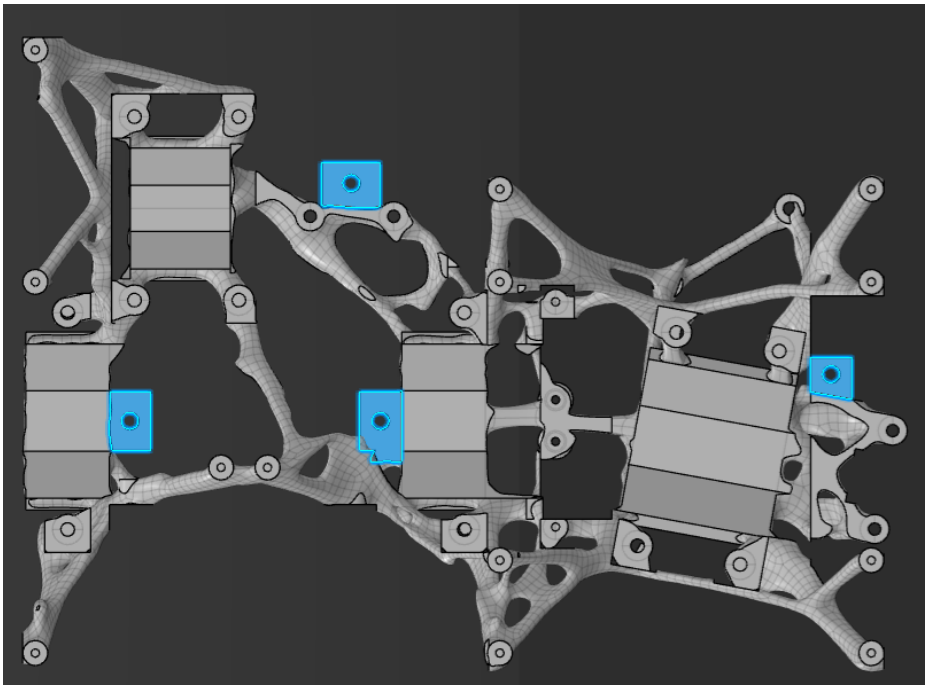

Figure 26: The four added fastening points for machining

5.7 The final part

The final part has a mass of 186g, and with the brackets and corresponding bolts the mounting solution has a total mass of 208g. This is down from 1124g for the HYPSO-1 design resulting in a 81.5% decrease in mass when brackets, bolts and dampers are included. The total mass of the payload is 1519g and the center of gravity of the satellite is (10.8mm, -2.6mm, -40.1mm) in the (x,y,z) directions, thus fulfilling **STRM-3-020** and **PLD-3-010**.

When it comes to tolerances the part had several faces that were significantly different from the intended geometry. In particular the grating cassette leading faces highlighted in Figure 27 are significantly off by being 0.5mm thinner than intended, meaning the surface is 0.1mm further in than the target surface after machining. There is also some warping on the v-grooves which resulted in the machining not being equal on both sides. This effect is depicted in Figure 28 where it can be seen that the machining is not equal on both sides of the groove.

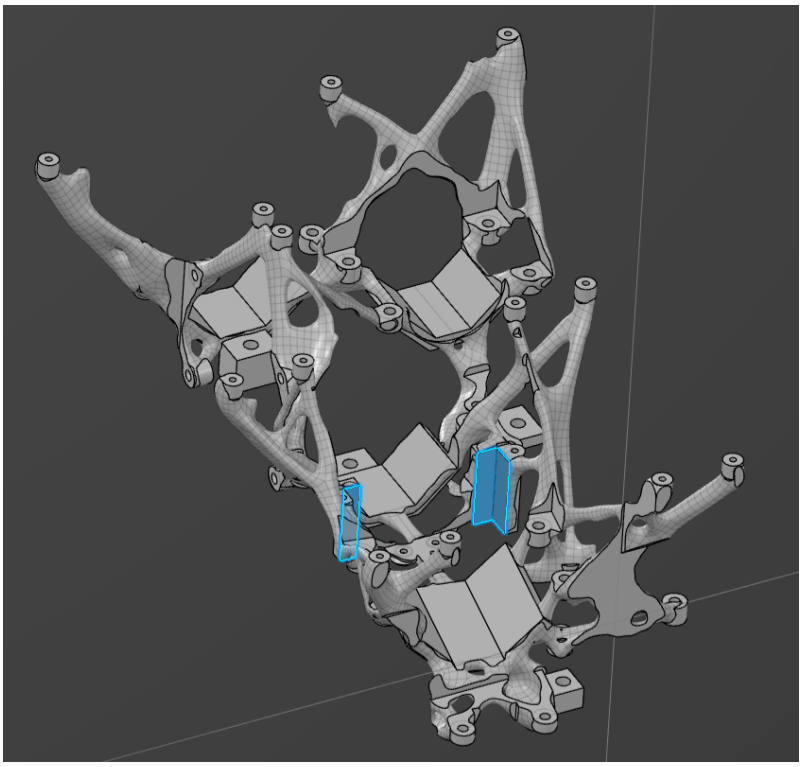

Figure 27: The grating cassette leading faces that are significantly offset

6 Discussion

6.1 Topology optimization

6.1.1 Function integration

The first step in the topology optimization was to create the design space and was done using the methodology laid out in section 2.4.1. This method enabled the design to both take into consideration the functional surfaces and requirements in a way that gave the maximum design space possible, thus giving the topology optimization the design freedom it needs to give good designs. The methodology also tied in manufacturing considerations from the start, in particular manufacturing direction is of importance, which makes sure that the design can ease manufacturing by for example limiting overhangs. The resulting design space was therefore free of any overhangs before beginning the optimization process.

Figure 28: The machined v-groove

6.1.2 Choice of strategy

When choosing a strategy for the optimization this process took longer than expected. This was due to the theoretically optimal strategy of using "minimize mass while respecting constraints" did not converge, neither for a stress nor eigenfrequency constraint.

To investigate the issue with the minimize mass strategy it was tested on a smaller and less complex component to test if the optimization procedure was set up correctly. This showed that the TO converged as expected, but only for a very fine mesh. It is therefore hypothesized that the reason this strategy did not work on a more complex and larger part is due to the mesh not being adequately refined compared to the magnitude of the load. This could be explained by imagining a cylinder with a load on one end and fixed in the other. As the TO reduces the mass this will at one point, if the load is sufficiently small compared to the element size, result in a cylinder with a diameter of one element having a lower stress than necessary to hit the requirements. This means the TO will continue to remove mass from the one element wide cylinder, resulting in the pseudo-density of the remaining elements to quickly approach zero mass due to the power law. This is also substantiated by the fact that the largest stresses observed were in the 6U frame and not on the optimized part, meaning the part could easily be reduced further below 5% while still maintaining the stress requirement. It is therefore concluded that too large elements likely is the main reason this optimization strategy did not work as intended.

This fault was attempted to be remedied by decreasing the element size, but this resulted in the solver not converging. Another option that was considered was to reduce the design space and element size, thus maintaining the same number of total elements, but this was not done due to the uncertainty of where the design space could be reduced without significantly worsening the optimization results.

Since "minimize mass while respecting constraints" did not converge, other strategies had to be attempted. The resulting strategy utilizing "maximize stiffness for a given mass" in an iterative fashion worked well for finding good designs. This strategy converged for a low target mass of 5% both without constraints and with an overhang constraint of 45° and therefore gave good weight reductions.

6.1.3 Setup and loads

The way the TO was set up worked well. The in built validation simulation setup meant that the inclusion of one side of the 6U frame shortened the time required for setup after each TO significantly.

The main drawback for the setup and loads was the fact that gravity loads did not converge. Instead a remote force in the center of gravity of each component was used. In the beginning this was thought to be a significant detriment to the simulations, but as it became apparent that the mass target could be set to 5% and give usable concepts this concern was lessened. It is therefore not thought that the lack of self-weight load significantly altered the TO results as the load missing represented an increase of 18% to the total load.

Another drawback was the lack of pre-tightening on the bolts. This resulted in the generated concept not sufficiently connecting the bracket mounting holes to the v-groove. In particular the RGB camera suffered from this as seen in Figure 15 (a). However this was not a major issue as this was easily remedied by manually connecting the two areas.

6.1.4 Results

By utilizing the iterative approach of continuously decreasing the mass target several concepts were generated. At the 5% mass target it can be seen that for both the no-constraint and overhang constraint concepts have local geometry that significantly lowers the eigenfrequency for all modes. This is to be expected based on the same reasoning for the "minimize mass while respecting constraints" since the mass target of 5% approaches the limit for how thin the geometry can be based on the element size. This therefore increases the likely-hood for errors in the geometry, which in turn causes the sharp change in eigenfrequency, stress and displacement. This can therefore be relatively easily be remedied using validation simulations followed by manual changes.

6.2 Shape review

The addition of the shape review steps shown in Figure 8 turned out to be crucial in getting the lightest concept possible. If the validation with subsequent manual changes had not been used then the last mass target to fulfill the requirements would have been the 7.5% concepts, adding 50% more weight to the part. Often the intricacies of design can be hard to quantify into constraints that a program can execute flawlessly. It is therefore important to keep in mind that TO is a tool to aid in finding material distributions that are beneficial, not necessarily to give the designer the most optimal design. Allowing manual edits to the optimization results can therefor in many cases give even more optimal results, either by accounting for requirements that can not be set into constraints or by fixing minor faults in the resulting topology.

6.2.1 Concept simulation

The concept simulations are for the most part identical to the TO simulations. However the main shortcoming of the TO setup has been addressed to improve the accuracy of the results. By switching from remote load to gravity load of 12g the concept simulations now account for the self-weight of the concept, thus giving more accurate results.

When it comes to the results from the simulations it is of note that simulating the unedited 5% with overhang constraint concept resulted in extreme values, particularly for stress and displacement, when compared to the other concepts. This is due to the simulation being linear, i.e. it does not account for plastic deformation, and can therefore continue to deform indefinitely. The area connecting the grating cassette holes to the rest of the part therefore create extreme values both in stress and displacement because of the very small cross-sectional area it has. These values are therefore within expectations due to the small cross-sectional area, resulting in very low stiffness

and high stress and displacement values. By adding stiffness to this area the part obtained much more reasonable and desirable values in the edited version, showing that the lack of stiffness in the area was the reason.

6.2.2 Manual changes

The manual changes was very effective at improving the simulated values. In particular the addition of material to fasten the grating cassette mounting holes was crucial in meeting the structural requirements for the two concepts. The addition of material between the bracket mounting holes and the v-groove was also effective at reducing the displacement, in particular for the RGB camera for the 5% concept.

This added mass was somewhat offset by the removal of areas that were deemed to give a low amount of stiffness, i.e. the long thin arms that were used for mounting to the 6U frame where thicker arms were close by. These were therefore deemed to not significantly impact any of the simulated metrics and were therefore removed. When simulating the edited concepts both showed an increased performance in all metrics, showing that the removed areas did not significantly reduce the performance. The removal of these arms also gave the benefit of reduced part count and reduced assembly time by removing one screw per arm removed.

6.3 Choice of concept

When choosing the final concept for the part it was considered to use a trade-off analysis to find the better part. This was however deemed unnecessary when there were only two concepts to choose from. A trade-off analysis usually performs better when there are many factors to account for and several options. As there were only two concepts a logical comparison was deemed sufficient. This comparison focused on the mass, displacement, eigenfrequency, stress and need for support. Ultimately the two concepts were almost equal in terms of mass-to-performance where the 5% overhang concept traded an increase in mass for increased stiffness. The deciding factor was therefore the need for support, which is highly correlated with cost as it adds a significant amount of post-processing. The slight increase in mass was therefore deemed worth it for the increased stiffness and reduced need for support when manufacturing the part.

6.4 Final result

The resulting part is the 5% overhang concept with the manual changes. This gave a part with the first eigenfrequency mode of 133Hz, max displacement of 0.212mm and max stress of 87.2MPa. This is therefore well within the requirements for the part with 0.212 mm displacement not being large enough to interfere with other parts during shock and vibration testing (**ENV-11**), 133Hz being above the required 74Hz (**ENV-10**), and the stress of 87.2MPa being below the max allowed of 150MPa (60% of yield strength, **STRM-3-016**). The mass for the part is also significantly improved, going from 1124g to 208g, giving a weight reduction of 81.5% compared to HYPSO-1.

After the part was produced the need for the machining became apparent. The warping was more significant than expected since the added 0.4mm was not sufficient to allow machining to the correct tolerance. The offset in the grating cassette mounting holes of 0.1mm means that the grating cassette might sit flush since that will roughly counteract the missing 0.1mm from the leading face.

When it comes to the v-groove this might need to be remedied. The uneven sides means that the objectives might not sit correctly, thus reducing image quality. This can be remedied by re-doing the machining where all three grooves are lowered by 0.5-2mm, depending on what is necessary. This will offset the HSI objective by an equal amount in the -Y-direction which will not impact the HSI performance. For 0.5mm the reduced thickness is negligible, but for 1-2mm reduction a new simulation would be needed to verify the structural integrity. The lowering should therefore

not be more than necessary to achieve good tolerances. In addition to the v-grooves the alignment faces for the two sensors would then also need to be lowered by an equal amount.

6.5 Additive manufacturing for CubeSats

When the metrics of the final part are considered it is clear that switching from a machined design to a design utilizing the capabilities of AM can bring great performance improvements. Especially TO is a useful tool in improving the mass-to-stiffness ratio of a part. As the mass in satellites is an important factor to costs it is an import factor to minimize, perhaps more so for CubseSats as these satellites are already limited in size and mass. By reducing the mass of the mechanical parts in a satellite more room is given for other components in the mass budget, allowing the other components to be heavier. This is especially useful for components such as batteries, where their performance is heavily tied to their weight. Topology optimization therefore brings out the potential in the design freedom enabled by AM to a great degree.

It is clear that the technology has significant benefits, but it also comes with some drawbacks. The main ones to note are in relation to manufacturing defects, mainly warping, porosities and residual stresses. Especially warping poses a significant risk as exemplified by the manufactured part. Warping will significantly alter the tolerances of the part and often only occur after the part is loosened from the supports. In some cases the part may even warp so much that it tears the supports or delaminates the part. Warping is mainly from residual stresses, meaning it is important to account for the dissipation of heat to minimize the residual stresses. The last significant material defect is porosities. This is especially common for metal AM where residual stresses can create pores as the material cools. These three defects therefore often appear simultaneously, reducing the reliability and tolerances of the part. Thermal management is therefore an important factor in mitigating risk when utilizing AM, and potentially thermal simulations to improve tolerances by adjusting the geometry based on the results.

7 Conclusion

This thesis set out to explore the use of AM in CubeSats by developing an additively manufactured part. This was done using TO to generate different concept shapes with lower and lower mass until the requirements no longer were met. This was followed by manual changes to the lowest mass concepts so they met requirements and could be utilized for the final design. By implementing a shape review process after the concept generation some of the shortcomings of TO could be addressed so that a better design could be achieved. This methodology was therefore highly effective at utilizing the capabilities of AM by optimizing the material distribution within the given design space. TO is therefore an excellent tool to use when developing CubeSats.

When it comes to the utilization of AM as a manufacturing technology for CubeSats the answer is not so clear cut. Here the designer needs to weigh the potential performance improvements that AM might give to the risks it comes with. In particular the risk for warping, residual stresses and pores are of significance. These risks must therefore be accounted for during the design of the part to minimize the risk of the part failing either during launch or while in space. Since repair or replacement of parts is impossible after the part is on the launch vehicle the designer might find that the risk outweigh the performance increase, resulting in AM not being suitable for that specific part. But in many cases the part may give significant performance increase while still being well within the requirements, meaning the risk of failure is minimal. By sufficiently testing the part as well the risk can be mitigated to such a degree that the performance out-weighs the risks. In this case the utilization of AM will be a feasible manufacturing technology when designing structural components for CubeSats.

7.1 Future work

As the developed part is as of now almost purely theoretical the future work revolve mainly around the simulation, testing and usage of the part developed. The following list summarizes the most crucial areas of work remaining before flight-readiness:

- Improve tolerances by re-doing machining or by re-producing the part with either extra thickness on machined surfaces or with adjusted geometry based on thermal simulation of the manufacturing process
- Simulate random vibration and shock to validate the vibration and shock response
- Do thermal simulations to verify thermal requirements
- Do an assembly and integration test to see that all parts fit as intended and that it does not interfere with the rest of the satellite
- Test the part for random vibration and shock to verify the structural integrity

In addition to the list above it might also be beneficial to do thermal analysis of the additive manufacturing process to correct the geometry based on the process parameters. This way the part warps into the correct geometry, thus improving tolerances and potentially removing the need for machining.

References

6082-T6 Aluminum (2022). *6082-T6 Aluminum :: MakeItFrom.com*. URL: https://www.makeitfrom.com/material-properties/6082-T6-Aluminum (visited on 23rd May 2022).

Ahmad, Abas, Michele Bici and Francesca Campana (Jan. 2021). 'Guidelines for Topology Optimization as Concept Design Tool and Their Application for the Mechanical Design of the Inner Frame to Support an Ancient Bronze Statue'. en. In: *Applied Sciences* 11.17. Number: 17 Publisher: Multidisciplinary Digital Publishing Institute, p. 7834. ISSN: 2076-3417. DOI: 10.3390/app11177834. URL: https://www.mdpi.com/2076-3417/11/17/7834 (visited on 23rd Feb. 2022).

Bendsøe, Martin P. and Ole Sigmund (2004). 'Topology optimization by distribution of isotropic material'. en. In: *Topology Optimization: Theory, Methods, and Applications*. Ed. by Martin P. Bendsøe and Ole Sigmund. Berlin, Heidelberg: Springer, pp. 1–69. ISBN: 978-3-662-05086-6. DOI: 10.1007/978-3-662-05086-6_1. URL: https://doi.org/10.1007/978-3-662-05086-6_1 (visited on 21st Feb. 2022).

Christensen, Peter W. and Anders Klarbring (2009). 'Topology Optimization of Distributed Parameter Systems'. en. In: *An Introduction to Structural Optimization*. Ed. by Peter W. Christensen and Anders Klarbring. Solid Mechanics and Its Applications. Dordrecht: Springer Netherlands, pp. 179–201. ISBN: 978-1-4020-8666-3. DOI: 10.1007/978-1-4020-8666-3_9. URL: https://doi.org/10.1007/978-1-4020-8666-3_9 (visited on 4th Feb. 2022).

Dev Singh, D., T. Mahender and Avala Raji Reddy (Jan. 2021). 'Powder bed fusion process: A brief review'. en. In: *Materials Today: Proceedings*. 2nd International Conference on Manufacturing Material Science and Engineering 46, pp. 350–355. ISSN: 2214-7853. DOI: 10.1016/j.matpr.2020.08.415. URL: https://www.sciencedirect.com/science/article/pii/S2214785320362878 (visited on 17th Dec. 2021).

Diegel, Olaf, Axel Nordin and Damien Motte (2019). *A Practical Guide to Design for Additive Manufacturing*. en. Springer Series in Advanced Manufacturing. Singapore: Springer Singapore. ISBN: 978-981-13-8281-9. DOI: 10.1007/978-981-13-8281-9. URL: http://link.springer.com/10.1007/978-981-13-8281-9 (visited on 24th Nov. 2021).

Dilip, J. J. S. et al. (Jan. 2017). 'Selective laser melting of HY100 steel: Process parameters, microstructure and mechanical properties'. en. In: *Additive Manufacturing* 13, pp. 49–60. ISSN: 2214-8604. DOI: 10.1016/j.addma.2016.11.003. URL: https://www.sciencedirect.com/science/article/pii/S2214860416301087 (visited on 15th Nov. 2021).

Durakovic, Benjamin (Dec. 2018). 'Design for additive manufacturing: Benefits, trends and challenges'. en. In: *Periodicals of Engineering and Natural Sciences (PEN)* 6.2. Number: 2, pp. 179–191. ISSN: 2303-4521. DOI: 10.21533/pen.v6i2.224.

EOS (2014). *EOS Aluminium AlSi10Mg Material Data Sheet*. URL: https://www.eos.info/03_system-related-assets/material-related-contents/metal-materials-and-examples/metal-material-datasheet/aluminium/material_datasheet_eos_aluminium-alsi10mg_en_web.pdf.

Frazier, William E. (June 2014). 'Metal Additive Manufacturing: A Review'. en. In: *Journal of Materials Engineering and Performance* 23.6, pp. 1917–1928. ISSN: 1544-1024. DOI: 10.1007/s11665-014-0958-z. URL: https://doi.org/10.1007/s11665-014-0958-z (visited on 3rd Nov. 2021).

Furger, Steve M (May 2013). 'Analysis and Mitigation of the CubeSat Dynamic Environment'. en. PhD thesis. San Luis Obispo, California: California Polytechnic State University. DOI: 10.15368/theses.2013.27. URL: http://digitalcommons.calpoly.edu/theses/1042 (visited on 18th Dec. 2021).

Gibson, Ian et al. (2021). *Additive Manufacturing Technologies*. en. Cham: Springer International Publishing. ISBN: 978-3-030-56127-7. DOI: 10.1007/978-3-030-56127-7.

Image Color Summarizer - RGB and HSV Image Statistics (2022). URL: http://mkweb.bcgsc.ca/color-summarizer/? (visited on 27th May 2022).

ISO/ASTM 52900:2015(E) Additive manufacturing — General principles — Terminology (Dec. 2015). URL: https://www.iso.org/cms/render/live/en/sites/isoorg/contents/data/standard/06/96/69669.html (visited on 2nd Nov. 2021).

Natural Frequency and Resonance (Nov. 2019). URL: https://community.sw.siemens.com/s/article/Natural-Frequency-and-Resonance (visited on 9th June 2022).

University, C.P.S. (June 2018). *6U CubeSat Design Specification Revision 1.0*. URL: https://static1.squarespace.com/static/5418c831e4b0fa4ecac1bacd/t/5b75dfcd70a6adbee5908fd9/1534451664215/6U_CDS_2018-06-07_rev_1.0.pdf.

Yang, Sheng, Yunlong Tang and Yaoyao Fiona Zhao (Oct. 2015). 'A new part consolidation method to embrace the design freedom of additive manufacturing'. en. In: *Journal of Manufacturing Processes*. Additive Manufacturing 20, pp. 444–449. ISSN: 1526-6125. DOI: 10.1016/j.jmapro.2015.06.024. URL: https://www.sciencedirect.com/science/article/pii/S1526612515000699 (visited on 9th Nov. 2021).

Yang, Sheng and Yaoyao Fiona Zhao (Sept. 2015). 'Additive manufacturing-enabled design theory and methodology: a critical review'. en. In: *The International Journal of Advanced Manufacturing Technology* 80.1, pp. 327–342. ISSN: 1433-3015. DOI: 10.1007/s00170-015-6994-5.

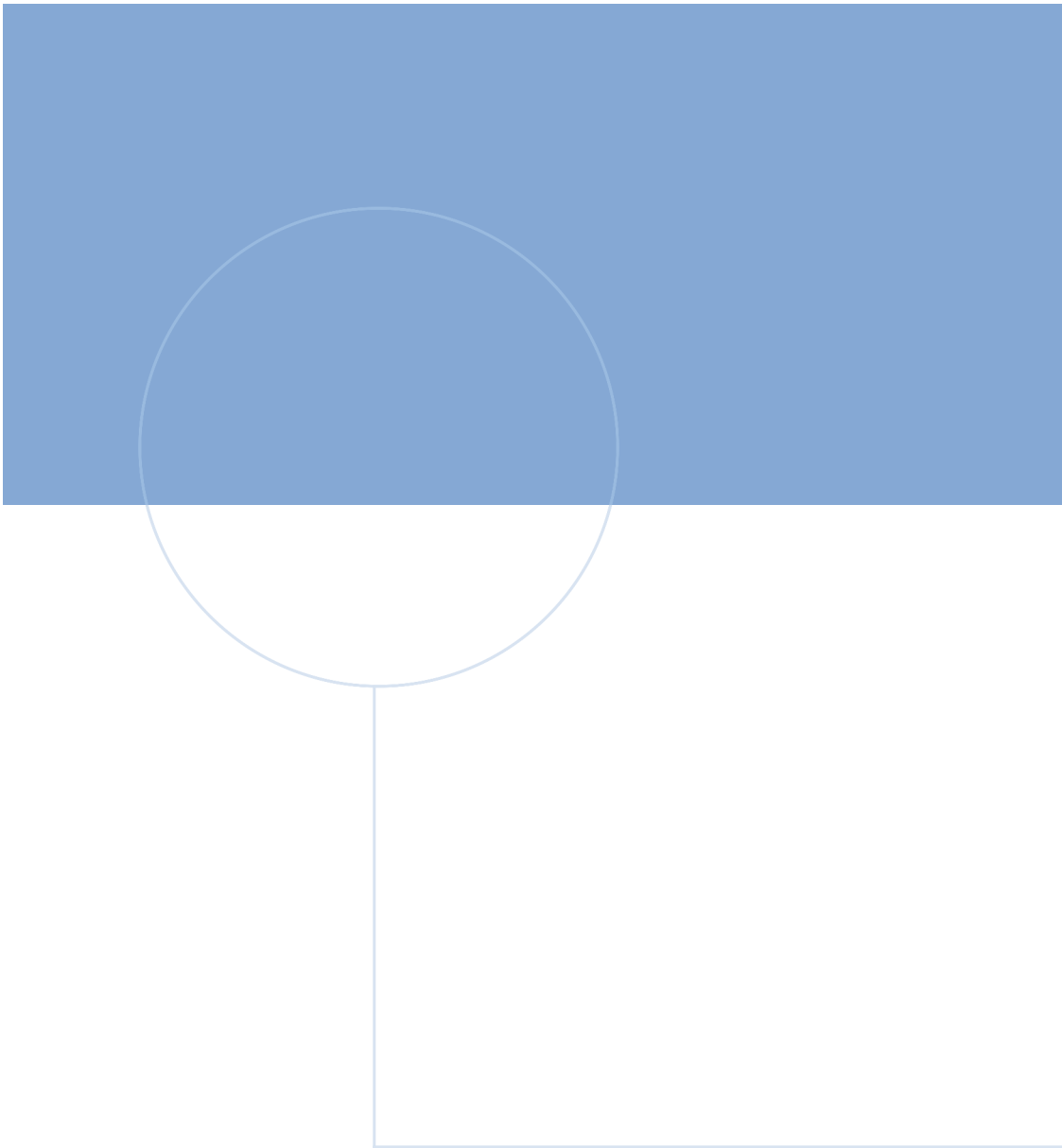

NTNU

Norwegian University of
Science and Technology